astrium GmbH	Technical Note	Herschel

Title: **HERSCHEL Straylight Calculation Results**

CI-No: 100 000

		Date:	
Prepared by:	Dr. A. Frey / *A. Frey* Dr. H. Hartmann *Ha*	Date:	21. 10. 02
Checked by:	Dr. E. Hoelzle		22. 10. 02
Product Assurance:	R. Stritter		22. 10. 02
Configuration Control:	A. von Ivády		24. 10. 02.
Project Management:	Dr. K. Moritz		25. Oct. 2002

Issue	Date	Sheet	Description of Change	Release
1	10.06.02	1-37	First issue	
2	18.10.02	1-74	Completely revised issue	

Table of contents

1   Introduction

This TN presents the results of the Straylight Analysis for HERSCHEL.

2   Reference Documents

RD1	Herschel Telescope Straylight Analysis	HER.NT.017.T.ASTR, issue 3, 01 Okt 02
RD2	Earth & Moon Radiometric Hypotheses for Straylight	H-P-ASPI-TN-0216, issue 1, 14 02 02

3 Straylight Requirements

The requirements as can be found in the IID-A, issue 2/0, are described below:

For the spacecraft design w.r.t. straylight for the Herschel instruments an integrated approach has been selected. This means that the instrument optical layout is included in the system straylight analysis. This approach allows to directly provide the straylight level originated from the various sources at the detector level.
The system straylight requirements are given therefore directly as the straylight reaching the detector level. The system will provide the following maximum straylight over the full operational wavelength:

Scattered light (source outside the telescope FoV)
Taking into account the worst combination of the Moon and the Earth positions w.r.t. the LOS of the telescope with maximal:
- Sun - S/C - Earth angle of 37°
- Sun - S/C - Moon angle of 47°
- Sun - S/C - LOS angle of 60° to 120°,
the straylight shall be: < 1.0% of background radiation induced by self-emission of the telescope.

Sources inside FOV:
Over the entire FOV at angular distances 3' from the peak of the point-spread-function (PSF), the straylight will be: $< 1 \cdot 10^{-4}$ of PSF peak irradiance (in addition to level given by diffraction).

Self-emission
The straylight level, received at the defined detector element location of the PLM/Focal Plane Unit Straylight model by self emission (with "cold" stops in front of PACS and SPIRE instrument detectors), not including the self emission of the telescope reflectors alone, will be 10% (tbc) of the background induced by self-emission of the telescope reflectors.

4   Model Description

4.1   General Overview

The present status of the overall ASAP model is displayed in fig. 4.1-1. A detailed plot of the design from the M1-baffle down to the instrument shield is shown in fig. 4.1-2.
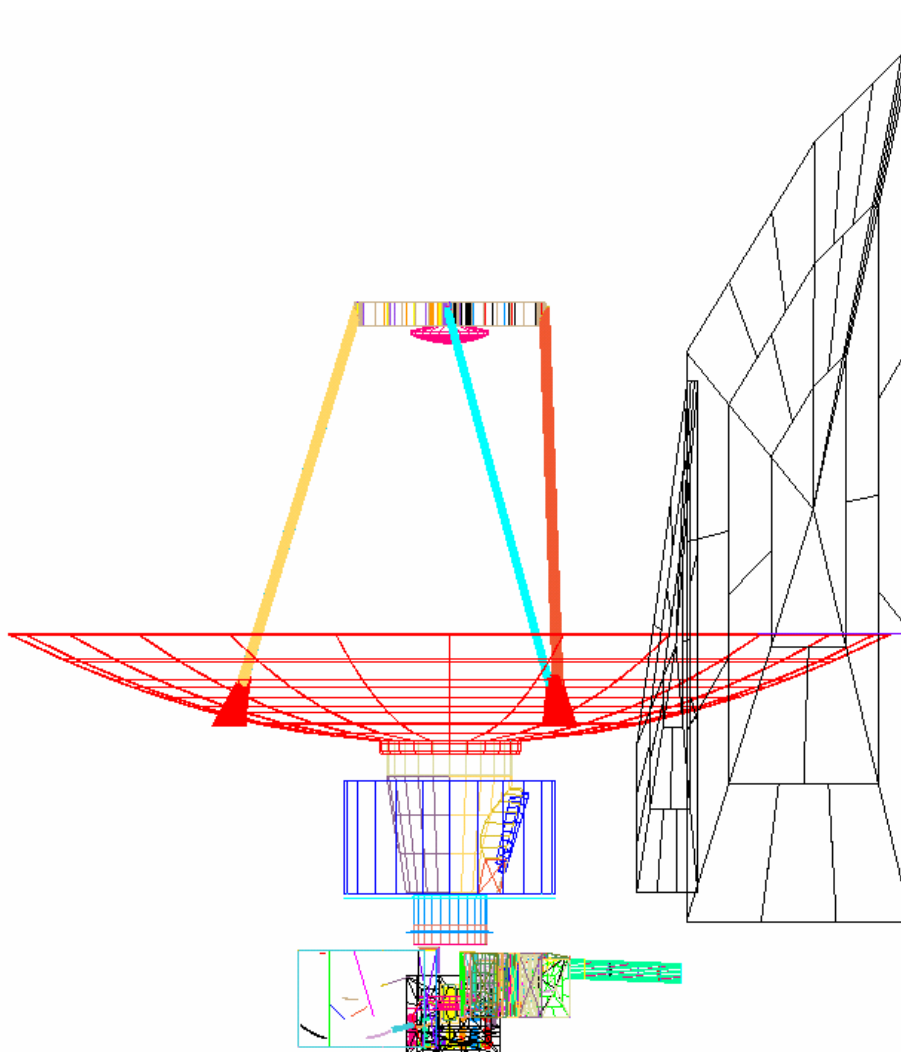
Fig. 4.1-1: Overall configuration plotted with the present ASAP model

cylindrical part of
M1-baffle

conical part of
M1-baffle within
cavity with cutouts
(left and right) for the
cryocover
mechanisms

CVV

heat shield 2
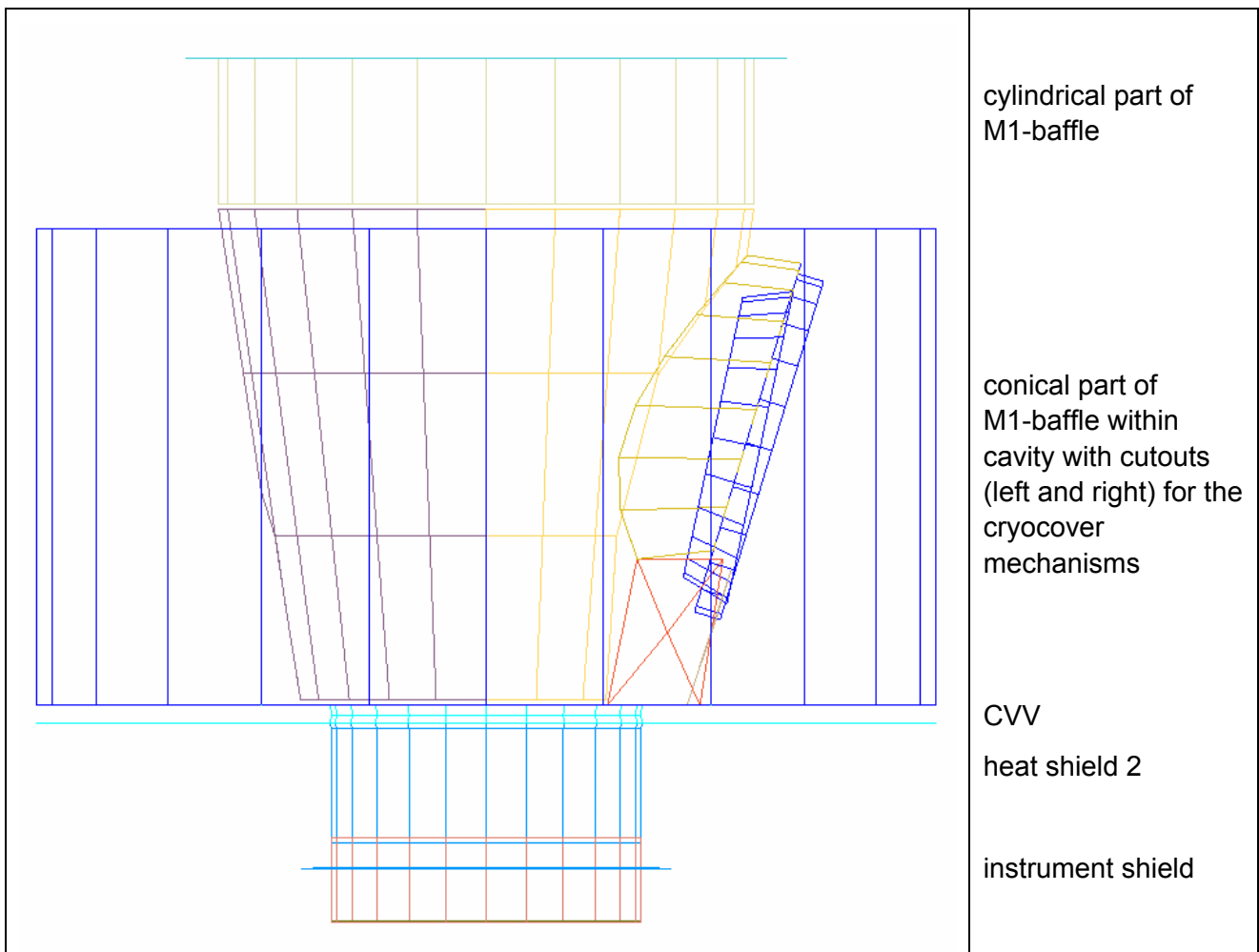
instrument shield

Fig. 4.1-2: Detail of design from M1-baffle down to the instrument shield

Four ASAP models have been received, all of them were integrated into the total optical ASAP model of Herschel
- the telescope model
- the SPIRE model
- the PACS model
- the HIFI-model (not yet included in issue 1 of this TN).

The rest of Herschel to be modeled for the straylight analysis comprises
- the sunshade
- the cryostat part near the cyrocover
- the baffle between cryostat and telescope (M1-baffle)
- the heat and instrument shields (the parts above the experiments).

Overview on the basis for the total model:

object	basis for modelling
OBA including instrument shield	drawing ref. no. HP-2-ASED-ID-0042-01-0A dated 18.10.02
PACS	ASAP Model from Kayser-Threde: file PACS-Top_Optics_Inside_11.inr (e-mail dated 27.03.02). model corrected and used by ASED: file PACS-Top_Opt_Ins_11korr.inr dated 26.06.02 contained in e-mail (dated 26.06.02) resent to Kayser-Threde
SPIRE	ASAP model from ESTEC/RAL files spire.inr, spire_macros.inr, spire_prop.inr, spire_scatter.inr, replacement_fp_unit.inr (e-mail dated 06.03.02) model corrected and used by ASED: file spire_tel2.inr dated 17.05.02 contained in e-mail (dated 17.05.02) resent to RAL/ESTEC
HIFI	ASAP model from ESTEC files HiFi.inr, hifi_ch1.inr, hifi_ch2.inr, hifi_ch3.inr, hifi_ch4.inr, hifi_ch5.inr, hifi_ch6.inr, hifi_ch7.inr, hifi_prop.inr, hifi_macros.inr, hifi_struct.inr (e-mail dated 27.11.01)
heat shield 2 baffle	ASED design to be incorporated in drawing to be issued
CVV	drawing ref. no. HP-2-ASED-ID-0039-01-0A dated 20.09.02 drawing ref. no. HP-2-ASED-ID-0004-01-0B dated 20.09.02 drawing ref. no. HP-2-ASED-ID-0009-01-0A dated 28.05.02
cryostat baffle (M1-baffle)	drawing ref. no. HP-2-ASED-ID-0039-01-0A dated 20.09.02 drawing ref. no. HP-2-ASED-ID-0009-01-0A dated 28.05.02
cryocover	drawing ref. no. HP-2-ASED-ID-0039-01-0A dated 20.09.02
telescope	ASAP model from ASEF (dated 26.05.02 by ASEF)
sunshade	doc. no. HP-2-ASED-IC-0002 issued 10.06.02

4.2 ASAP experiment models

The experiment ASAP models are displayed in the next figures:

- the SPIRE model in figure 4.2-1
- the PACS model in figure 4.2-2
- the HIFI-model in figure 4.2-3.

Several iterations have been performed for the SPIRE and PACS in order to have sufficient model fidelity. Final confirmation from the instrument teams not yet received.

ASAP-SPIRE-MODEL **M4+M4-aperture** **FP_UNIT**

=chopper **REF=0.3**
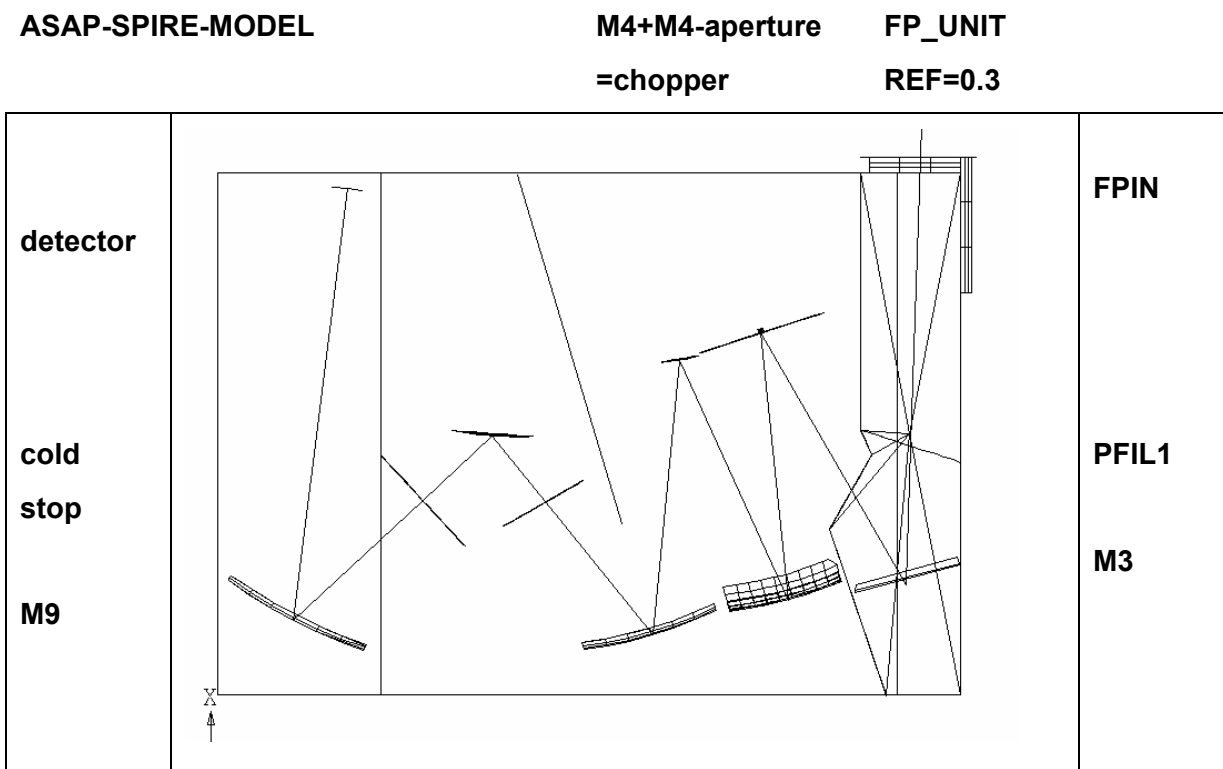
Figure 4.2-1:   ASAP SPIRE model; it represents a singular path towards one of the detectors of the photometer. This photometer path is representative for the straylight sensitive paths within SPIRE.

ASAP PACS-MODEL→cold stop   chopper

PACS CENTRAL RAY UP TO PACS FOCUS   640.16,939

X
Y
Z
-45.9941,4.43883,108.867 mm   ASAP

top-optics   'investigate'   detector

Figure 4.2-2:   ASAP PACS model. Only the optics is shown, without structural elements. A specific detector path has been selected as representative for straylight.

Compartments: **2**   **5**   **towards M2** ↑

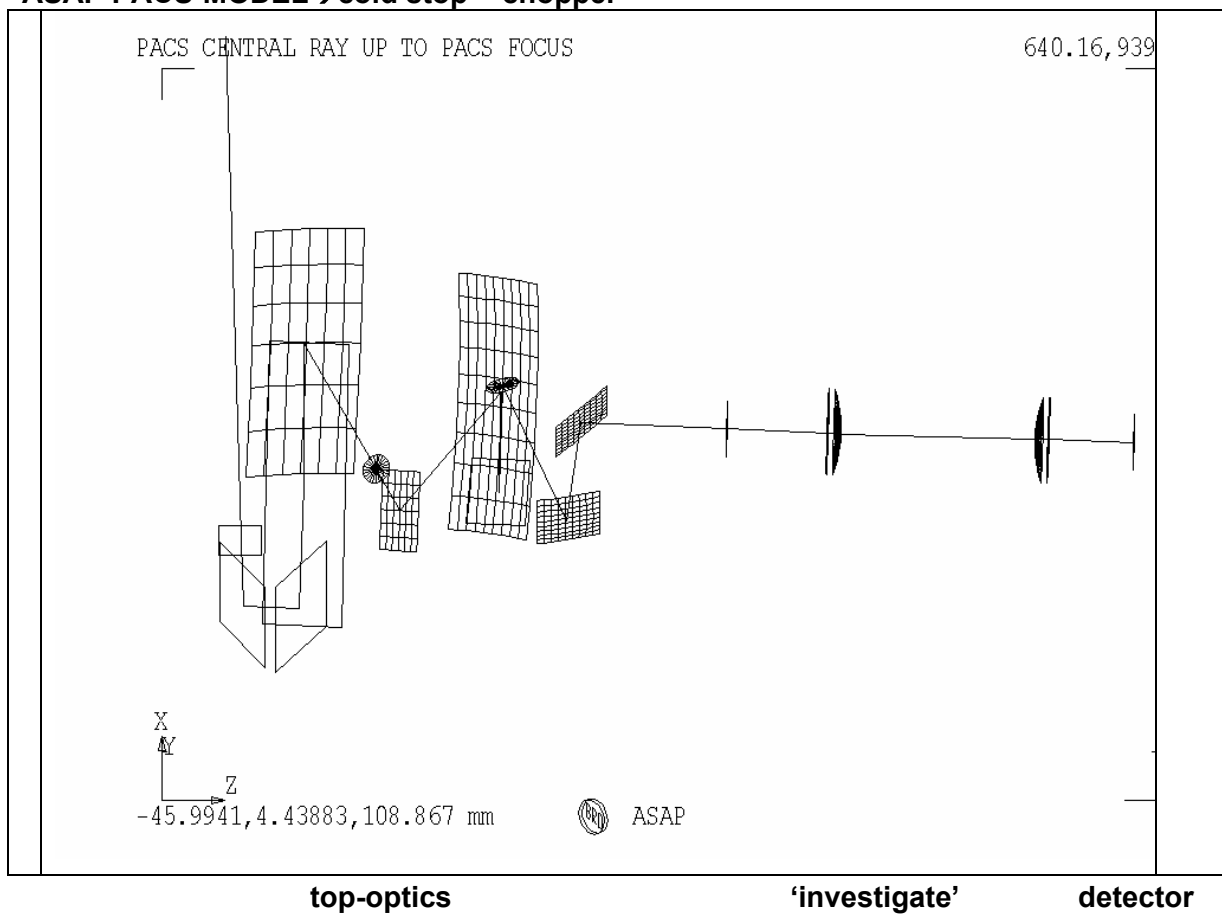**Compartments:**   **1**   **3**   **4**   **M3** ↑
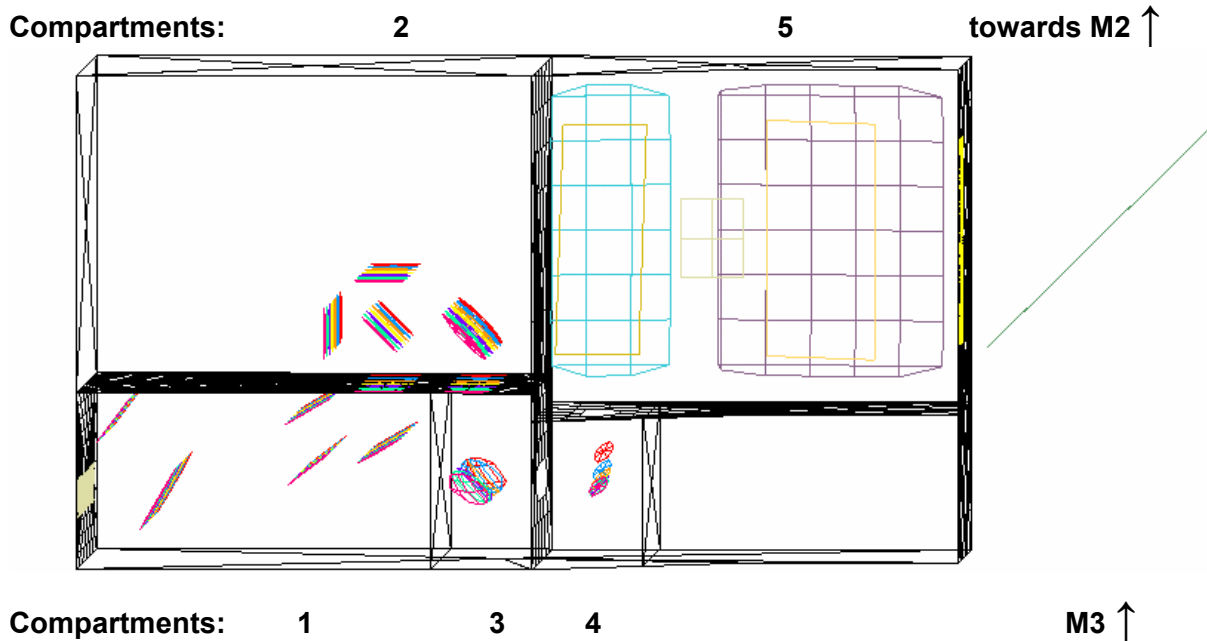
Figure 4.2-3   ASAP-HIFI model. HIFI is not straylight sensitive; it is included because it may influence straylight towards PACS and SPIRE. The compartment numbering is introduced in order to enable easier description of the straylight calculations. The compartment numbers increase from the local oscillator windows to the inner opening towards M3 and M2 (telescope secondary mirror).

There is an object-image relation between the hole within SPIRE M4 and the center of M2. This leads to a partial obscuration of some straylight contributions, as the calculations will show.

The optics design of SPIRE confines the acceptance cone for purely specular radiation very closely to the secondary mirror as a backward raytrace shows, only a very small fraction of the hexapod can be seen by the SPIRE detector (see figure 4.2-4).

SPIRE FIELD 8 X 4 ARCMIN ON M2, BACKWARD_TRACE   831.261,1002.5
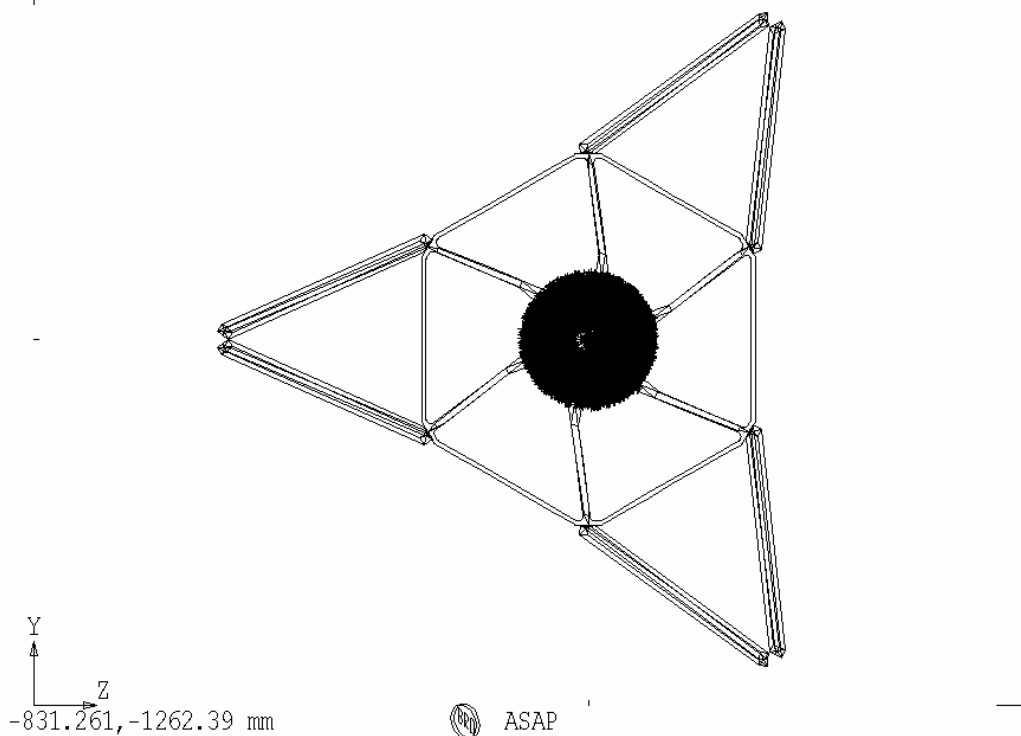
Y

Z

-831.261,-1262.39 mm   ASAP

Figure 4.2-4:   Backward trace onto M2 starting from the SPIRE detector

The confinement of the acceptance cone for purely specular radiation is similar for PACS (not as close as for SPIRE); a backward trace from the PACS detector is shown in figure 4.2-5.

PACS FIELD 3.5 X 3.9 ARCMIN ON M2, BACKWARD_TRACE   831.261,1002.5

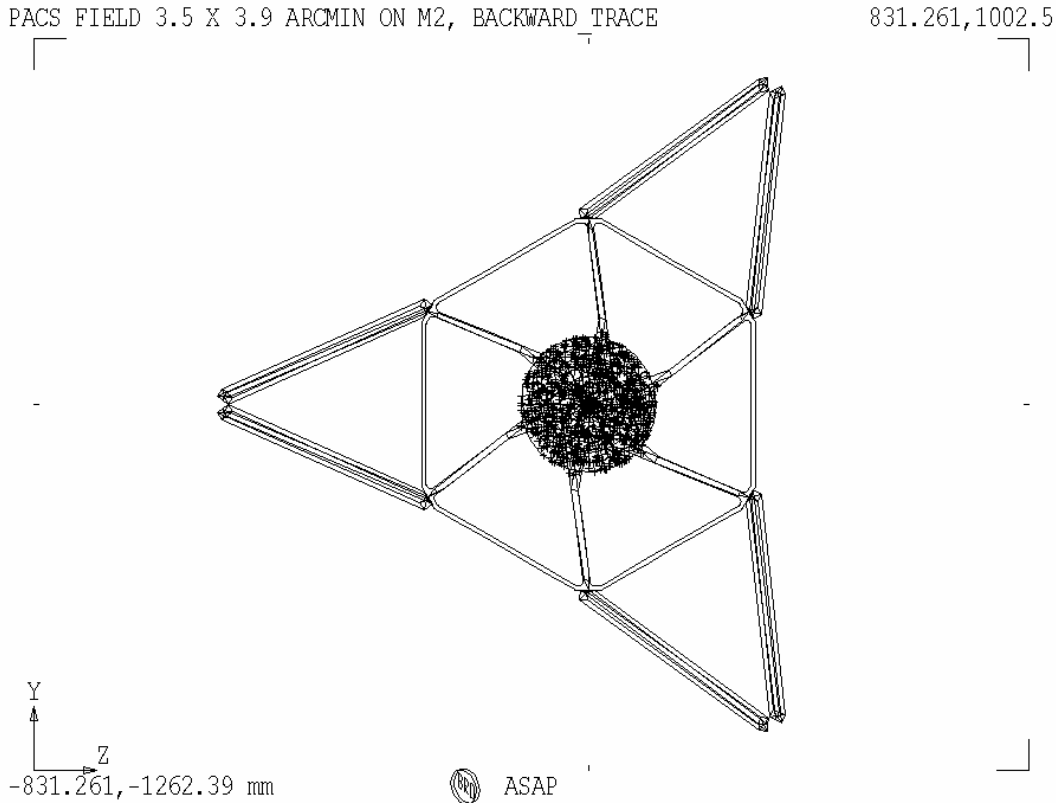-831.261,-1262.39 mm   ASAP

Figure 4.2-5:   Backward trace onto M2 starting from the PACS detector

For the straylight calculations the following instrument detectors have been considered as representative for all detectors of the respective instrument:
- SPIRE   SPIRE.optics.detector, (see figure 4.2-1)
- PACS: PACS.investigate.detector, (see figure 4.2-2).

A new addition w.r.t. issue 1 of this TN is the apodization effect (or edge taper) of the horns in front of the SPIRE detectors. For radiation impinging on the horns, this effect produces a change in sensitivity depending on the angle w.r.t. the horn axis such that the sensitivity decreases for increasing angles. Projected onto the pupils of SPIRE (cold stop, telescope secondary) there is a decrease of 8 dB, i.e. an edge taper of 8 dB. This edge taper is realized for the calculations with the apodization function of ASAP, this is a ray change in ASAP. Thus there is no change of objects in the ASAP SPIRE model. The effect of the ASAP apodization is displayed in fig. 4.2-6. This is not just a graphical representation of a gaussian function, but the result of a raytrace with a beam starting at the telescope secondary and ending at the SPIRE detector. There the resulting radiant intensity (in direction cosine space) is displayed without and with apodization. All the new calculations in this issue 2 (i.e. those on thermal self emission) have been performed including the apodization for SPIRE.

DIRECTIONAL SENSITIVITY OF SPIRE DETECTOR

FLUX / STERADIAN for A=.997
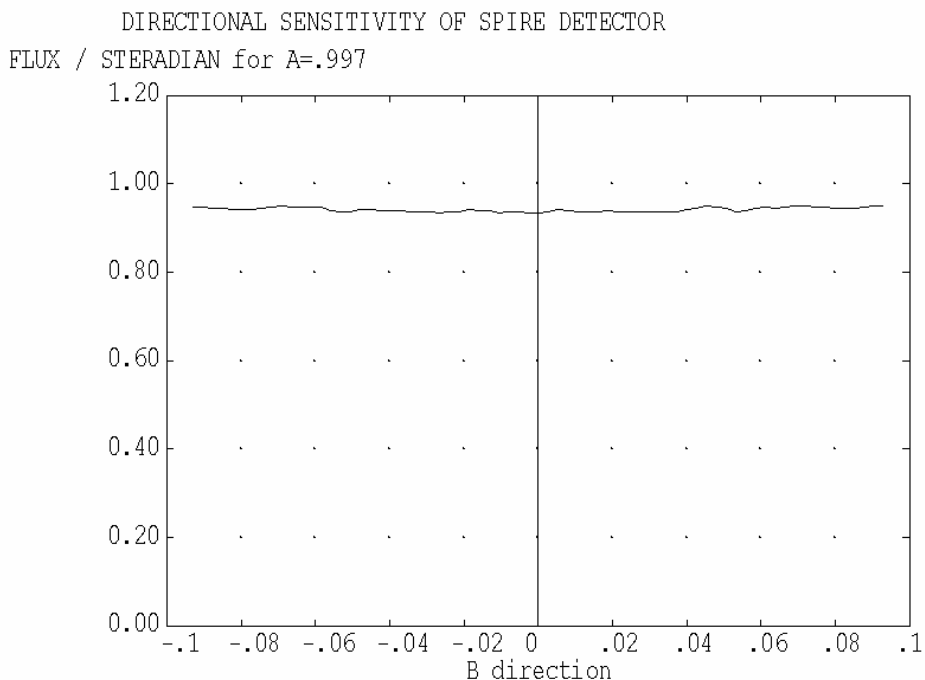
B direction

ABSCISSA IS DIRECTION COSINE SPACE
CURVE WITHOUT APODIZE FUNCTION FOR DIRECTIONAL SENSITIVITY

DIRECTIONAL SENSITIVITY OF SPIRE DETECTOR

FLUX / STERADIAN for A=.998
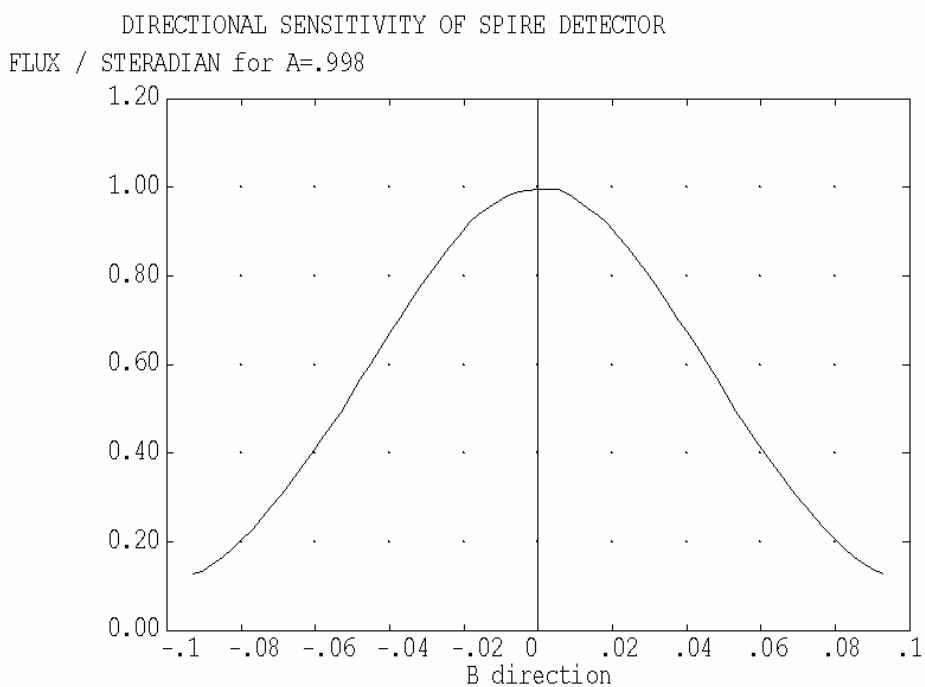
B direction

ABSCISSA IS DIRECTION COSINE SPACE
CURVE WITH APODIZE FUNCTION FOR DIRECTIONAL SENSITIVITY

Fig. 4.2-6:   ASAP apodization function at SPIRE detectors (edge taper of 8 dB)

The scattering functions of the experiments are grouped into 2 categories:
- scattering function for mirrors
- scattering function for thermal filters.

Those for the mirrors were found within the delivered ASAP files. It will become clear later on that they do not play an important role, i.e. mirror scattering within the experiments does not dominate. Therefore the choice of parameters is not important.

The SPIRE mirror scattering function is displayed in figure 4.2-7. It is a particle model with many parameters determining the resulting scattering function.

Two PACS mirror scattering functions have been delivered; as a worst case, the higher one has been selected (displayed in figures 4.2-8 and 4.2-9).

No scattering functions were delivered for thermal filters. For PACS, also the scattering functions for thermal filters are considered not important, as a check we inserted an (arbitrarily selected) high function, i.e. a lambertian scatterer with BSDF=0.1/π 1/sr at the place of the cold stop. No important scatter path resulted from this insertion.

For SPIRE the same scattering function was inserted for the thermal filters 1 and 2. Here the thermal filter 1 may open important scattering paths as the chapters on thermal self emission will show. It is therefore highly important to get knowledge on the scattering function of filter 1. If our selection is not a worst case selection, then the corresponding scatter paths will increase, especially for the case of a black cryocover.

There are two reasons for the imbalance between SPIRE and PACS with respect to the sensitivity on filter scattering
- the PACS thermal filter is more deeply buried within the experiment than thermal filter 1 of SPIRE
- the PACS opening is at a lower position (-X) than that of SPIRE,

both reasons lead to a higher irradiation of the SPIRE thermal filter 1.

PARTICLE   model

LOG BSDF

Angle: 1= 0.0 2= 30.0 3= 60.0
% TIS: 0.0284   0.0328   0.0562
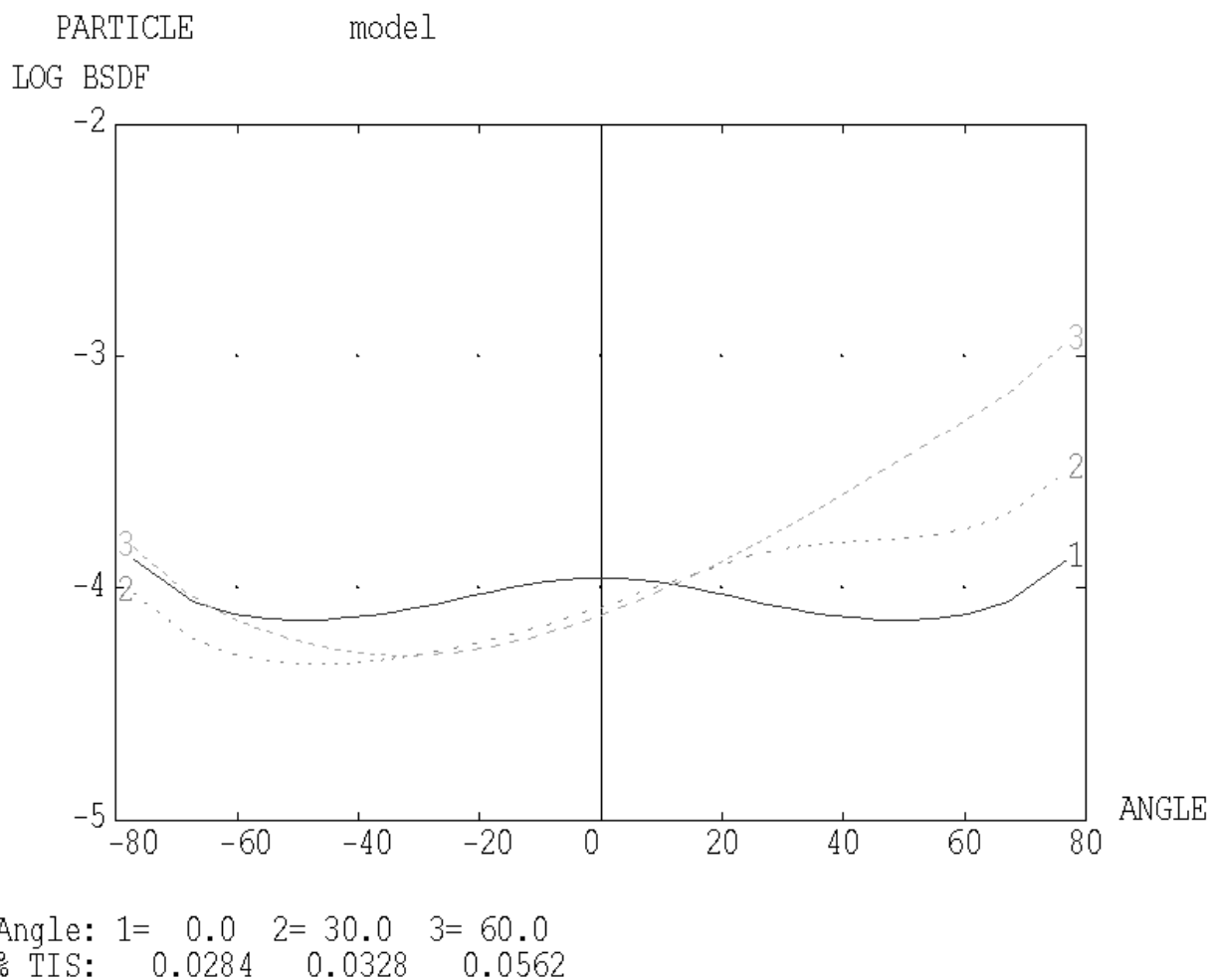
Figure 4.3-7:   Particle scattering function delivered with the SPIRE model for mirrors.

```
      HARVEY           model
    LOG BSDF
    -1
```



```
    Angle: 1= 0.0  2= 10.0  3= 20.0
    % TIS:   0.7249   0.7202   0.7058
```

Figure 4.3-8:   PACS mirror model with b(Harvey)=0.05, m(Harvey)=-2, shoulder 0.1. This figure mainly shows the characteristics at small angles.

HARVEY　　　　　model

LOG BSDF

Angle: 1= 0.0   2= 10.0   3= 20.0
% TIS: 0.7249   0.7202   0.7058

Figure 4.3-9:　　　PACS mirror model with b(Harvey)=0.05, m(Harvey)=-2, shoulder 0.1. This figure mainly shows the characteristics at large angles.

4.3   Telescope model

The telescope models were established by Astrium France, they are described in detail in reference document RD1. Some characteristics and the evolution of changes are repeated here for sake of completeness.

The telescope model now contains the variants
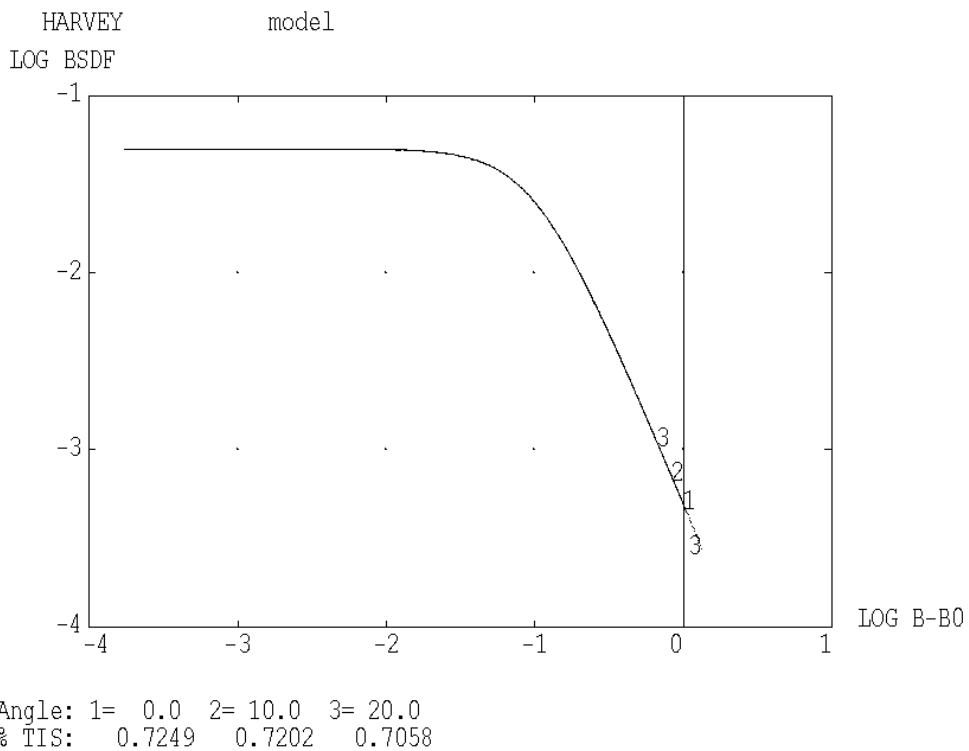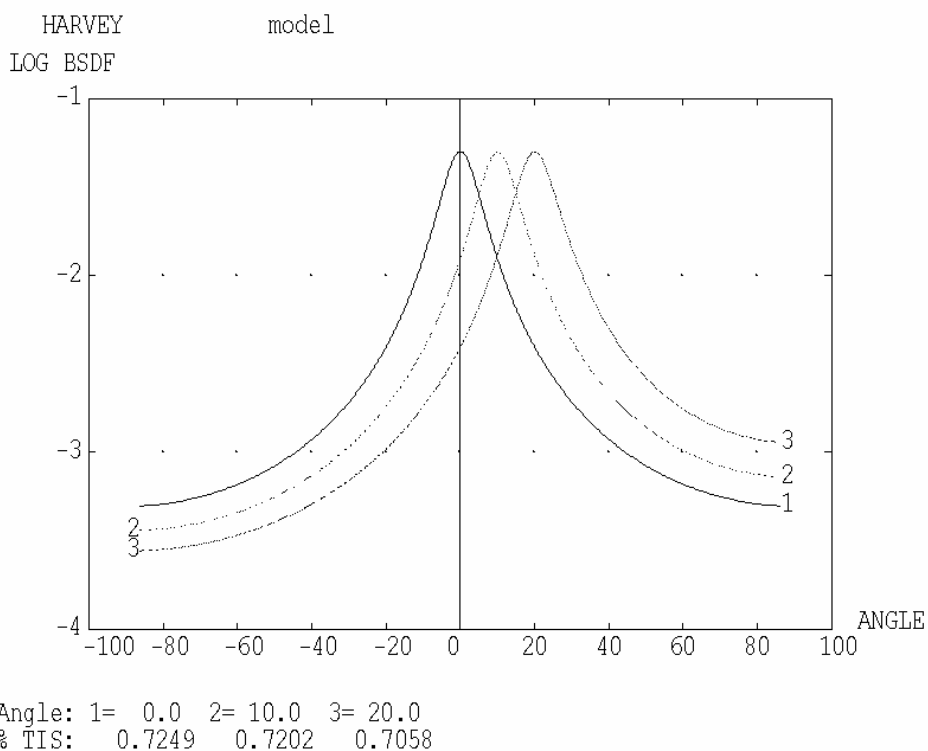- hexapod struts with rectangular struts
- hexapod struts with elliptical struts
- small scattercone with continuous slope change
- large scattercone with continuous slope change.

The rectangular struts were included in the calculations of issue 1 of this TN. Highly effective specular paths towards selected patches of the sky were detected for the rectangular struts. Therefore the version with elliptical struts was introduced, it shall reduce these specular paths. The elliptical struts are modelled with a polygonal cross section with 24 sides. All the new calculations in this issue 2 (i.e. those on thermal self emission) have been performed with the version with elliptical struts.

The scattercone (also called antinarcissus) was introduced earlier as a reflector placed in the center of the M2 mirror with an extent such that it occupies the area which cannot be used by the Cassegrain telescope type for stellar radiation (central obscuration). The slope had been devised such that backreflections from experiment to experiment/M1-baffle via M2 do not occur. As consequence there was a discontinuous slope change from the M2-surface to the surface of the scattercone. While that discontinuity is favourable for avoiding views of the experiments towards the objects in the center of M1 (via M2), it is likely to produce problems for HIFI in terms of standing waves.

Therefore versions of the scattercone with continuous slope change shall replace the version with discontinuous slope change. The different versions have the following properties

scattercone	central obscuration	standing waves	straylight
small discontinuous	lower	present	lower
small continuous	lower	reduced	higher
large continuous	higher	reduced	lower

Numbers for obscuration and straylight characteristics are listed in sections 5 and 6. Here the reflection behaviour of the three scattercone versions are displayed by the sequence of figures 4.3-1 through 4.3-3. There beams have been generated originating within SPIRE and PACS, these beam were traced backwards towards the M2-assembly. Similar figures have been presented in RD1 for the center of the FOV at the telescope system focus. The figures shown here use the following extreme beams from the edges (at –Z and +Z) of the SPIRE and PACS fields.

	color code in figures 4.3-1 through 4.3-3	
color	beam generated at	beam reflected by
blue	SPIRE, -Z side	scattercone, half at -Z
yellow	SPIRE, -Z side	M2, inner part near scattercone at –Z
black	PACS, +Z side	scattercone, half at +Z
red	PACS, +Z side	M2, inner part near scattercone at +Z

All the new calculations in this issue 2 (i.e. those on thermal self emission) have been performed with the versions with continuous scattercone (small and large).

A very recent improvement is the abolishment of the chamfers at the transition between scattercone and M2-surcface. These chamfers having the shape of a roof with 45 degrees inclination introduces a retroreflection in one plane. It was possible to sort out the most important of these paths before finishing this issue 2, so the effect of the chamfers is not present within the results on thermal self emission presented later on (the model still contains them).
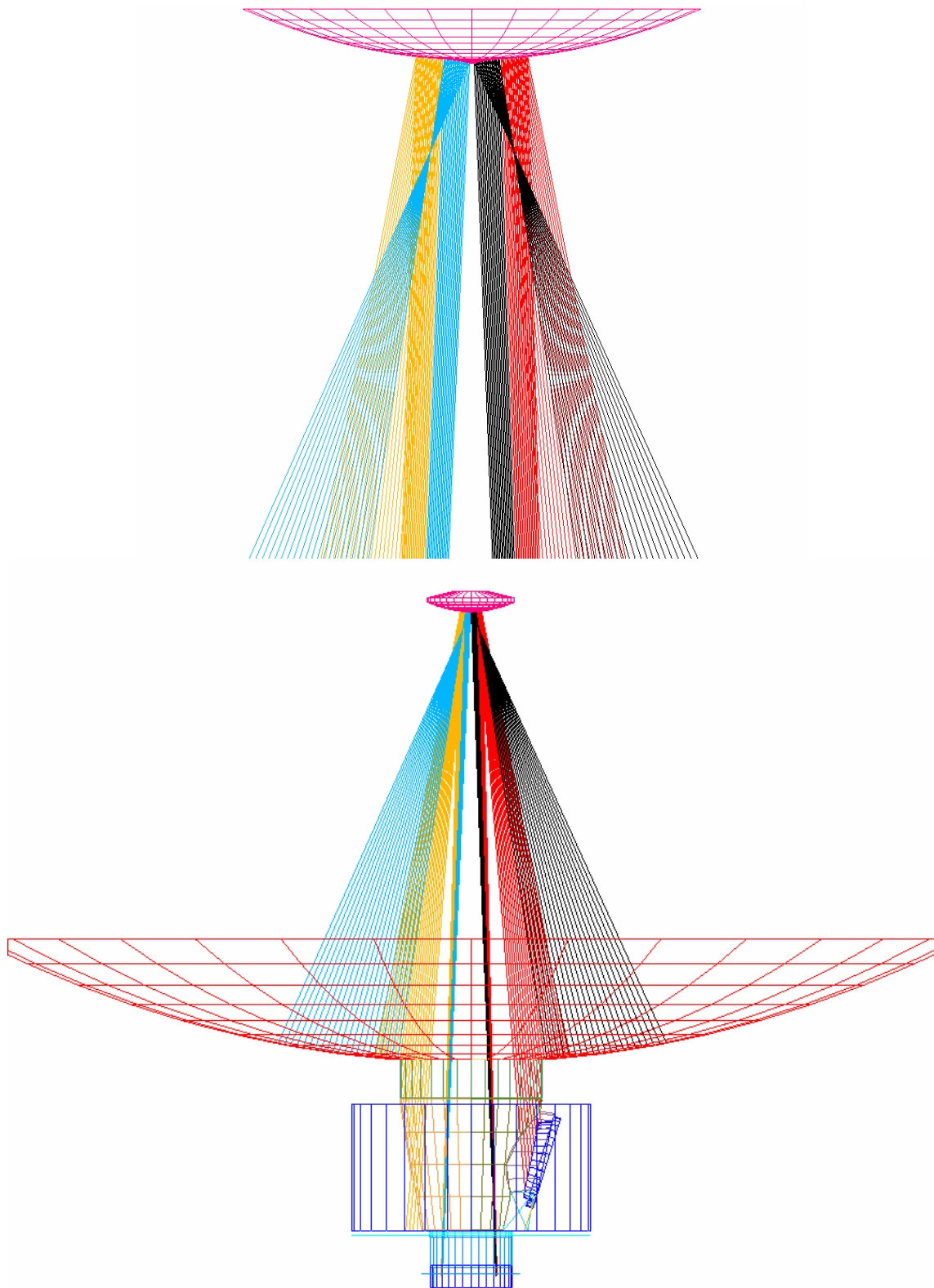
Fig. 4.3-1: Back-reflections by the small discontinuous scattercone
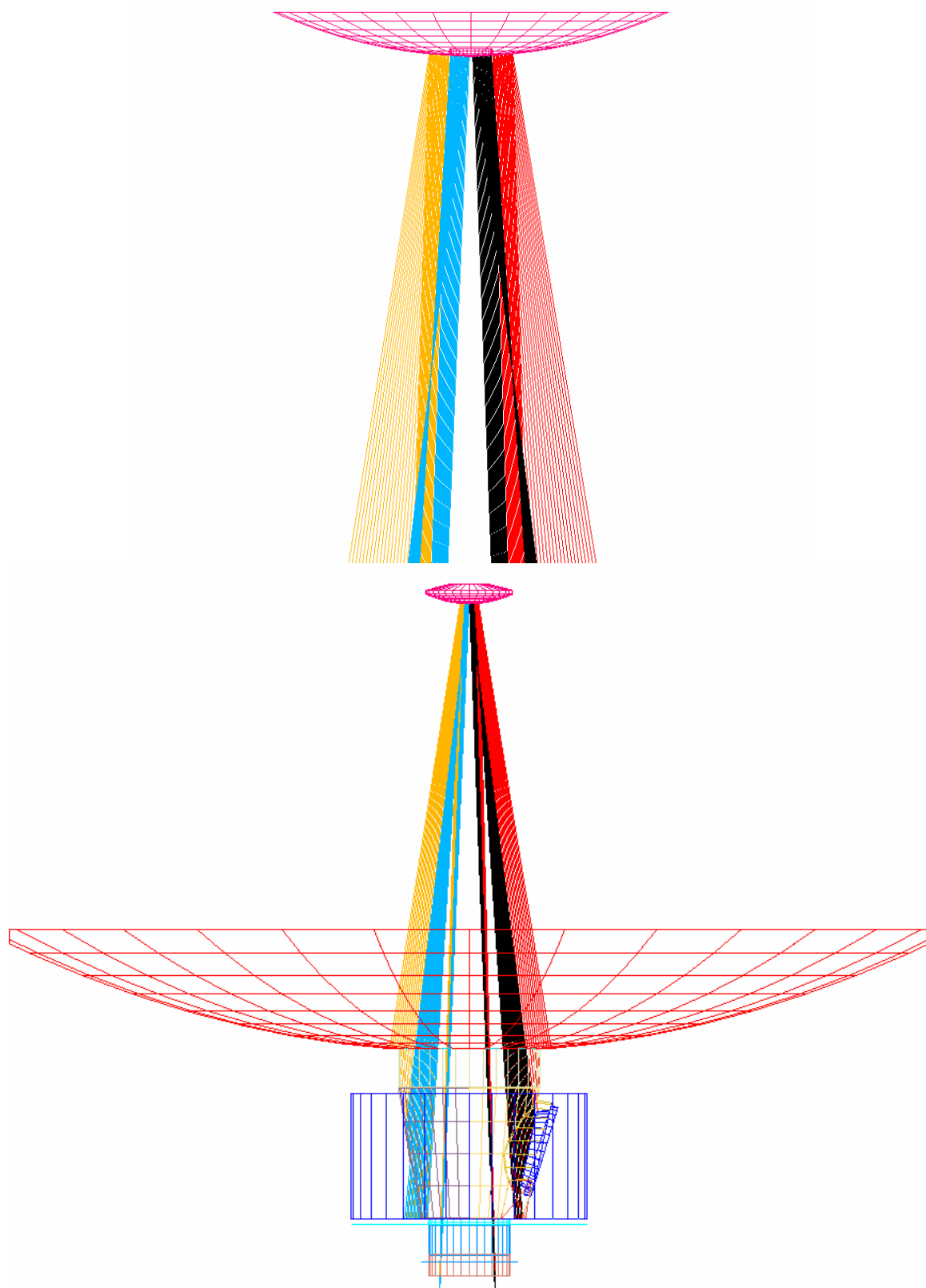
Fig. 4.3-2: Back-reflections by the small continuous scattercone
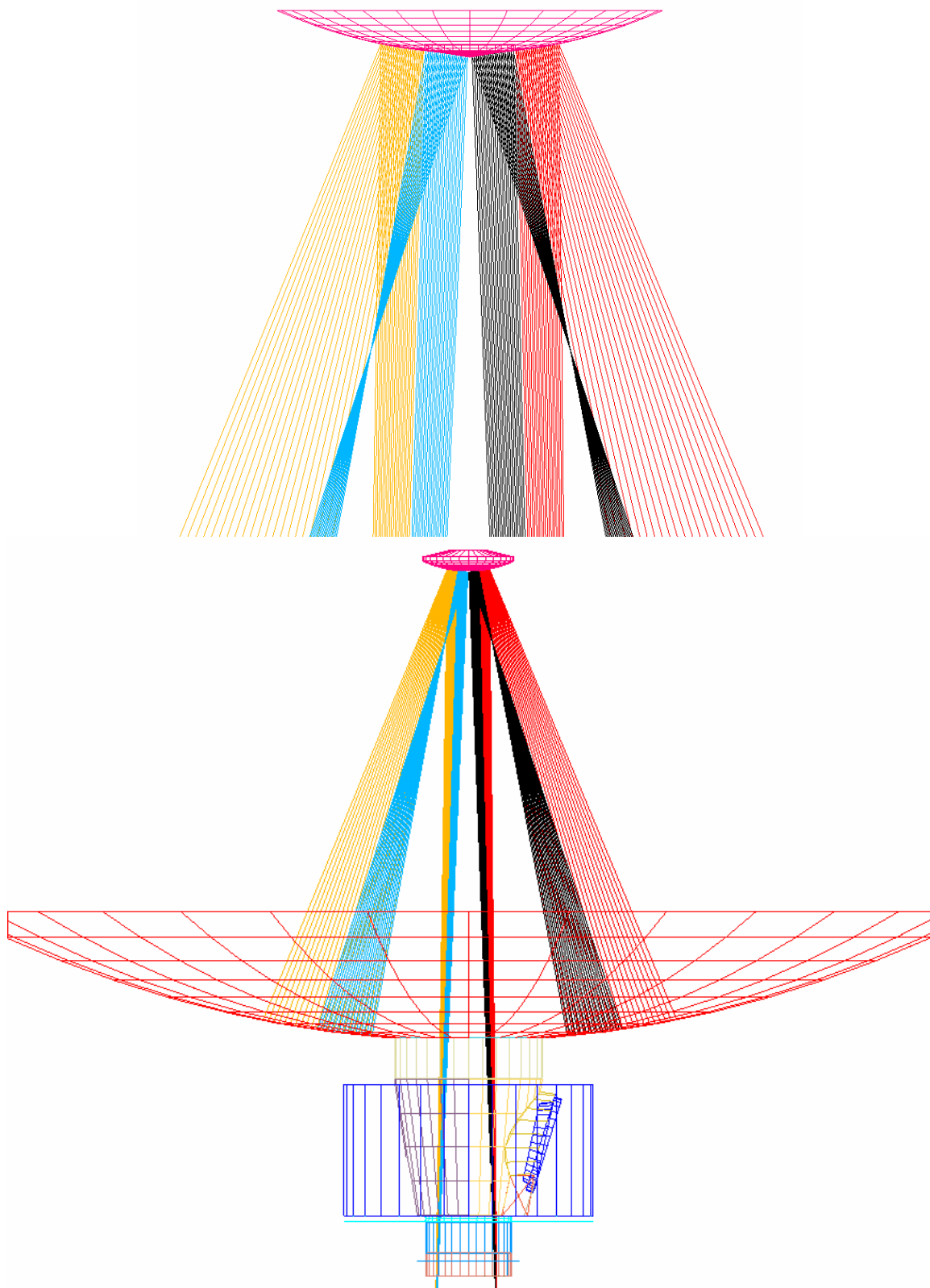
Fig. 4.3-3: Back-reflections by the large continuous scattercone

The telescope mirror scattering functions are displayed in the next series of figures. The roughness effect is shown in the figures 4.3-4 and 4.3-5.
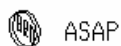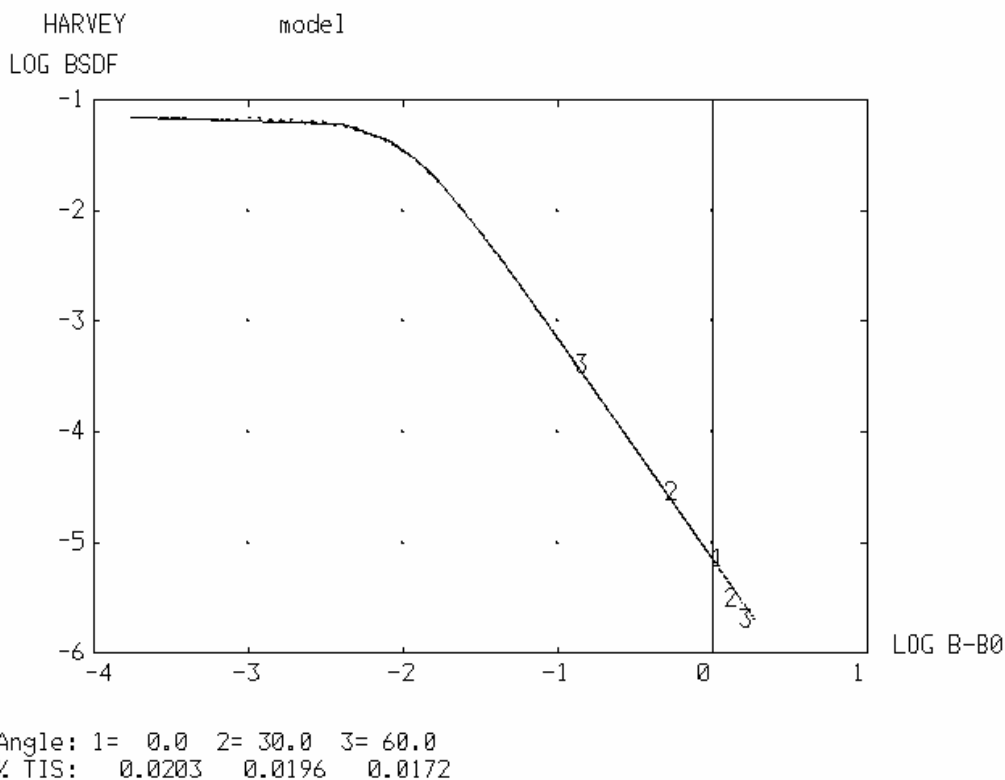
Figure 4.3-4:   Scattering function delivered with the telescope model: b(Harvey)=0.07, m(Harvey)=-2, shoulder 0.01. This figure is characterizing roughness. It mainly shows the characteristics at small angles.

```
HARVEY         model
LOG BSDF
```

Angle: 1= 0.0 2= 30.0 3= 60.0
% TIS: 0.0203   0.0196   0.0172

ASAP
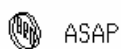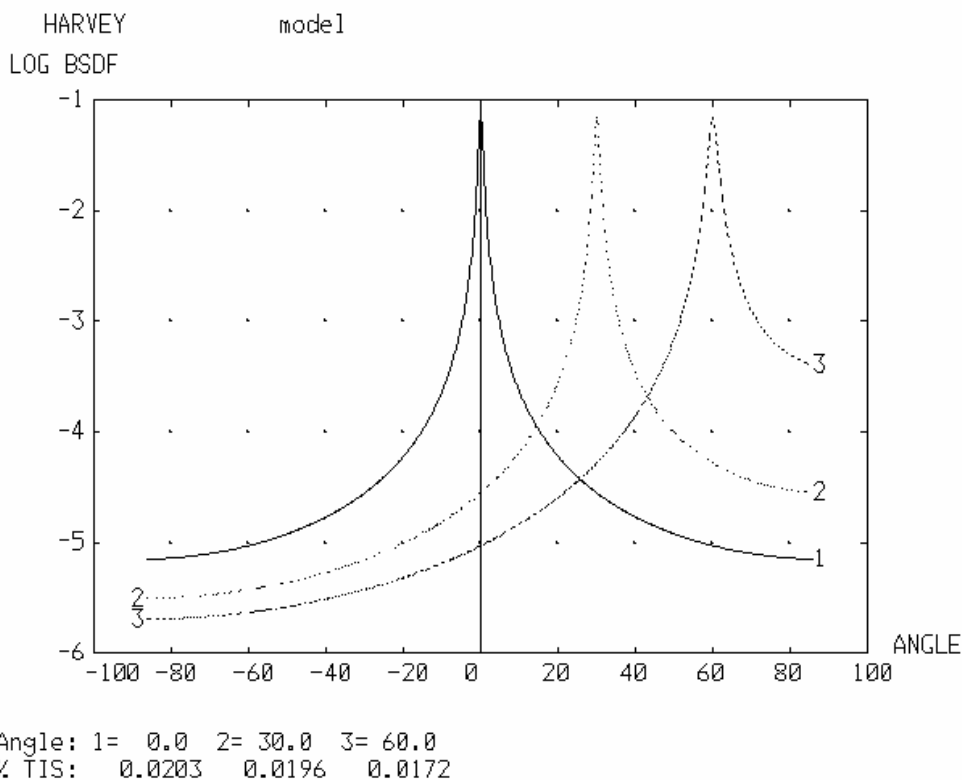
Figure 4.3-5:   Scattering function delivered with the telescope model: b(Harvey)=0.07,
                 m(Harvey)=-2, shoulder 0.01. This figure is characterizing roughness. It mainly
                 shows the characteristics at large angles.

For the contamination on the mirrors (presently to be assumed to correspond to particles with 5000 ppm) an extrapolated Harvey function has been presented (figures 4.3-6 and 4.3-7).
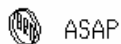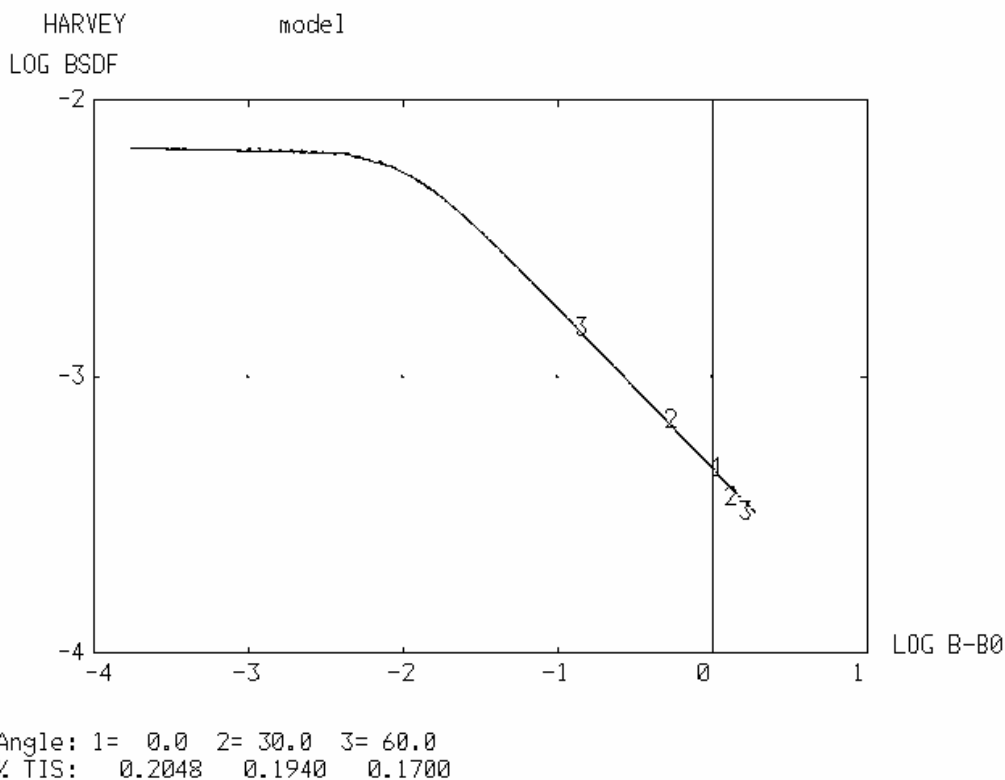
Figure 4.3-6:   b(Harvey)=6.7E-3, m(Harvey)=-0.58, shoulder 0.01 (extrapolation from10 to 85 micrometer, 5000 ppm). This figure mainly shows the characteristics at small angles.

```
        HARVEY        model
     LOG BSDF
```

Angle: 1= 0.0 2= 30.0 3= 60.0
% TIS: 0.2048   0.1940   0.1700
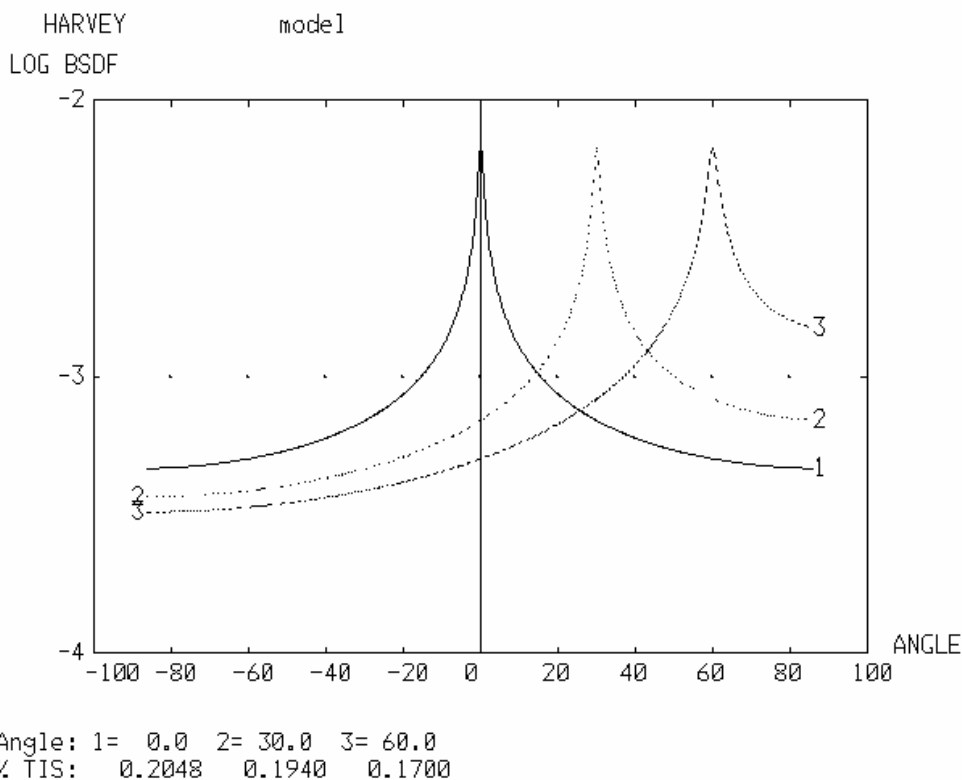
ASAP

Figure 4.3-7:   b(Harvey)=6.7E-3, m(Harvey)=-0.58, shoulder 0.01 (extrapolation from 10 to 85 micrometer, 5000 ppm). This figure mainly shows the characteristics at large angles.

Doc. No: HP-2-ASED-TN-0023   Page: **28**
Issue: 2   of: **73**
Date: 21.10.02   File: HP-2-ASED-TN-0023_2.doc

A comparison with the ASAP particle model which is used in the SPIRE model shows that the particle model delivers even lower BSDF values for contamination, especially for small angles. Nevertheless, the contamination model of figures 4.3-6 and 4.3-7 were selected, since the BSDF for roughness dominates anyhow, so actually the choice is not important. The contamination Harvey function is more easily to handle within ASAP than the particle model.

The Harvey function used in the calculations therefore is the sum of the two Harvey models

Effect	Harvey parameter b	Harvey parameter m	shoulder
Roughness	b=0.07	-2	0.01
contamination	b=0.0067	-0.58	0.01

A very recent change is the new scattering function for the telescope mirrors found in RD1:

	Harvey parameter b	Harvey parameter m	shoulder
	b=0.73	-1.7	0.01

This change will be included in further issues. The function is considered as a sum value containing both roughness and contamination.

4.4   M1 Baffle

The space between the hole within the primary mirror and the cryostat requires attention, since an interface harmonization was necessary there (keyword M1-baffle). The design follows the rules:
- keep warm bodies far off the experiment beam
- avoid zigzag reflections with directions roughly parallel to the x-axis

Zigzag reflections near the y/z-plane are not as critical as they are not likely to reach the experiments. The mechanical needs result in some planes parallel to the Y/Z-plane (e.g. on top of the CVV), so some zigzag reflection paths cannot be avoided.

Also other components around the baffle set constraints, mainly the cyrocover and the accessories necessary for its operation. The lower radius of the M1-baffle reflects the mechanical configuration there.

In issue 1 investigations have been performed for two different designs for the baffle within the centre of the telescope primary mirror (the M1-baffle),
- a cone-baffle
- a cylinder-baffle.

The progress in interface definition w.r.t. the inner rim of the telescope primary led to a restriction of the available diameter of 500 mm for the M1-baffle. Therefore a cylindrical shape has to be chosen for the upper part of the M1-baffle, since a continuous cone from the M1-vertex down to the CVV is not reasonable with an upper diameter of only 500 mm. The lower part can be made conical, the conical shape limits the thermal radiation transport towards the experiments. The resulting cone/cylinder-baffle has been shown already in figure 4.2-1. All the new calculations in this issue 2 (i.e. those on thermal self emission) have been performed with that version of the M1-baffle.

Several gap closures have been introduced around the (open) cryocover. Thus the so-called 'inner cavitiy objects' (which have been treated in issue 1 as highly emissive objects) now mostly are low emissive objects, only a small ring around the cryocover has to be treated as highly emitting.

There has been some discussion on the placement of the cryocover relative to the other Herschel components. Present status on object positions is
- sun/earth/moon and sunshade at +Z
- cryocover and main mechanics at +Z
- rest of cryocover mechanisms at -Z
- PACS at +Z
- SPIRE at –Z.

The chopping beam motion of the experiments is desired to occur with as much homogeneous background as possible. Therefore the chopping motions are parallel to the X/Y-plane with no appreciable beam motion towards Z. The cryocover position at +Z complies with that intention. The consequence is a possible misbalance of straylight onto PACS and SPIRE from the thermal emitters mentioned.

The surface of the cryocover is desired to be black for establishing a predictable background for the ground tests, baseline at PDR was a reflecting surface. The consequences for a black cryocover in terms of straylight will be highlighted.

4.5   Dimensions used

The most important dimensions as used in the ASAP model are shown in the following table:

Item	Dimensions
radius of small scattercone	16.5 mm
radius of large scattercone	36 mm
Z-distance of sunshade	1844 - 12 mm for MLI = 1832 mm
cylinderbaffle radius	250 mm
cylinderbaffle height (in X)	141 mm
width (in X) of gap between cylinder- and conebaffle	5 mm
conebaffle upper radius	250 mm
conebaffle lower radius	180.8 mm
conebaffle height (in X)	452.85 mm
CVV height (in X)	17 mm
width (in X) of gap between CVV and heat shield 2 baffle	8 mm
minimum inner radius of CVV and heat shield 2 baffle	144 mm
height of heat shield 2 baffle	98.1 mm
minimum inner radius of instrument shield baffle cylinder	144 mm
height of instrument shield baffle cylinder	73.4 mm

The lower end of the cylinder/cone baffle is 10 mm above the CVV plate. The large width of 8 mm (in X) of the gap between CVV and heat shield 2 is determined by the bending of the CVV ring under ambient pressure with vacuum below.

4.6   Emissivities and temperatures used

Item	Emissivitiy	Temperature
sunshade	0.05	204 K*
Gap between sunshade and M1	0.9	204 K*
telescope mirrors	0.015	70 K
M1-baffle	0.05	75 K
gap between cylinder- and cone baffle	0.9	75 K
cryocover	0.80	75 K
reflecting objects around cryocover	0.05	75 K
CVV	0.05	75 K
gap betw. CVV and heat shield 2 baffle	0.9	60 K
heat shield 2 baffle	0.8	43 K
instrument shield baffle cylinder	0.8	12 K

*Note on sunshade temperature: According to latest information, the worst case temperatures (EOL, hot case) will be for the central panel 200 K, + 14 K uncertainty, and for the side panels 180 K, + 14 K uncertainty. As we did not distinguish between central panel and side panels in our calculations, we here inserted an average worst case temperature of 204 K.

One should emphasize that this is a worst case temperature EOL. Most of the observing time, including hot case BOL will exhibit much lower temperature.

Emissivities of most objects are rough estimates only. They are based on worst case assumptions up to now, not on real measurements.

5   Supplementary Calculations

The obscuration effect on throughput for the different versions of the scattercone and the struts is cited from a calculation in RD1:

obscuration ratios	rectangular struts	elliptical struts
small scattercone	7.7%	8.7%
large scattercone	10.3%	11.3%

The obscuration effect on resolution is given in figures 5-1 through 5-3. The ascending curves represent the encircled energy in percent. The curve for the unobscured pupil (fig. 5-1) is given as test for the ASAP routine used for the calculation. The ASAP result is 86% encircled energy at the first dark ring while the theoretical value is 83%; this excess is an artefact of the generation of the figure, i.e. an peculiarity of ASAP. Thus the following figures should be regarded keeping in mind that the values of ASAP are too high by about 3%.

The values for the small and large scattercone are 82% and 78% encircled energy at the first dark ring (figures 5-2 and 5-3).
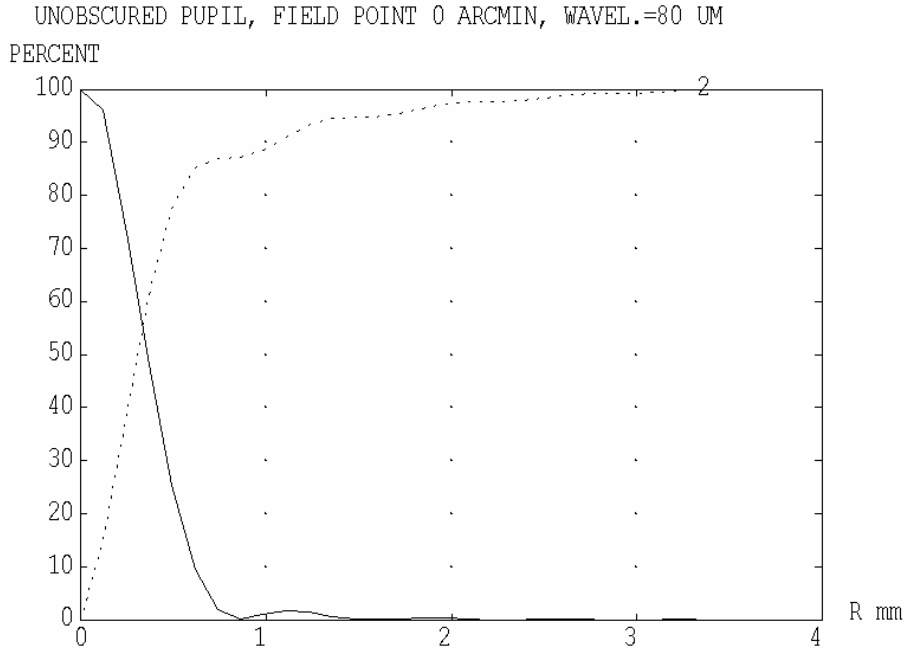
Figure 5-1: Radial energy distribution and encircled energy for an unobscured pupil.

RADIUS(ANT.NARC.)=16.5, FIELD POINT 0 ARCMIN, WAVEL.=80 UM

Figure 5-2: Radial energy distribution and encircled energy for an obscuration with a scattercone with radius 16.5 mm.

RADIUS(ANT.NARC.)=36, FIELD POINT 0 ARCMIN, WAVEL.=80 UM
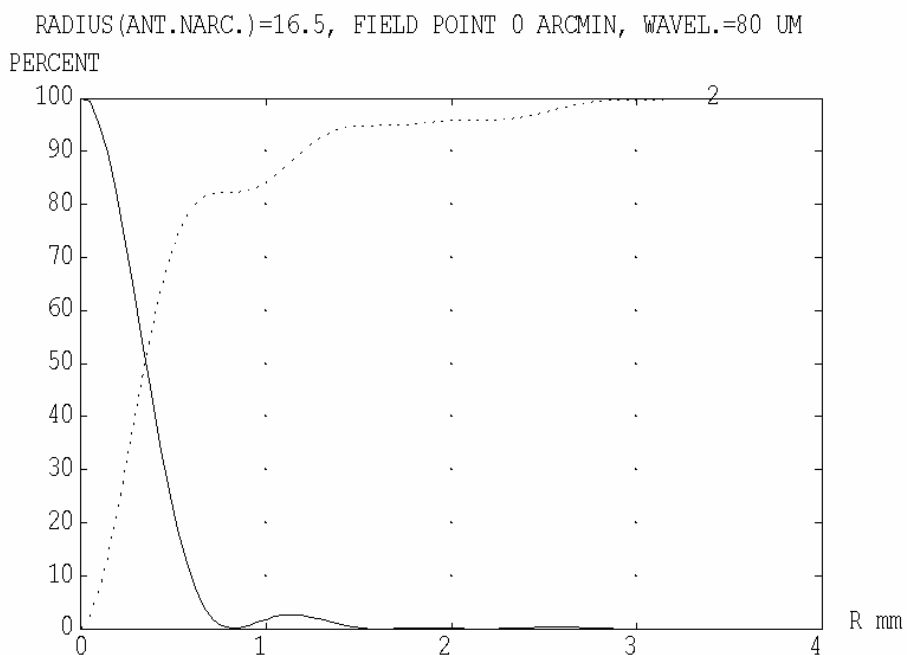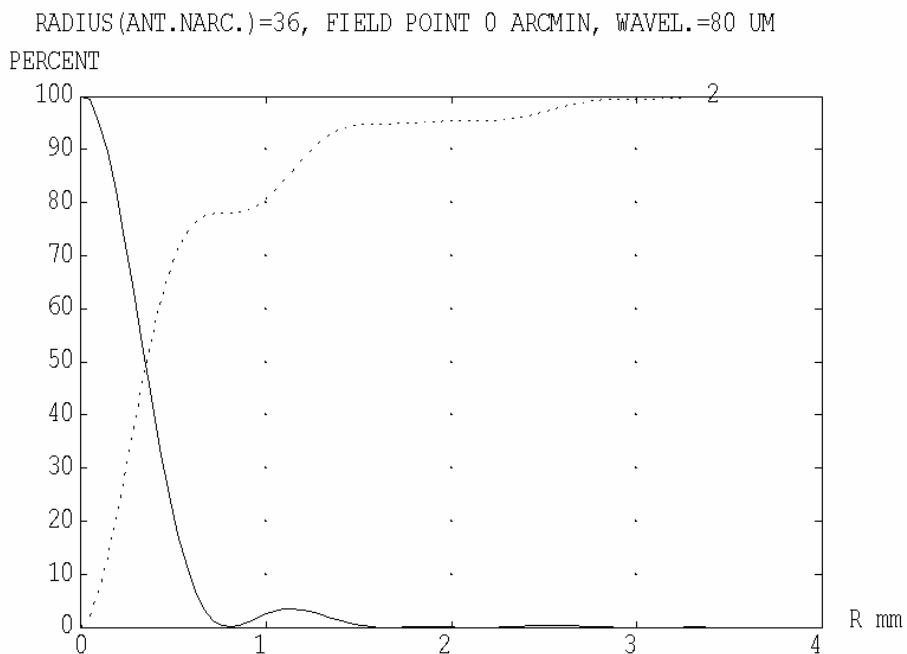

Figure 5-3: Radial energy distribution and encircled energy for an obscuration with a scattercone with radius 36 mm.

6   Thermal emission (Self emission)

6.1   Introduction

For most of the emitting objects, the purely specular paths are the dominant ones. The standard raytrace commands of ASAP have been used for the calculations.

The scattering functions mentioned in section 4 have been used for those cases where scattering is important (mirrors, filters). The scattering calculations require the definition of a solid angle into which the scattering occurs. For reasons of disk storage and calculational speed, this solid angle is limited as found necessary.

There are no standard ASAP commands available for all cases of diffraction. Therefore the diffraction is calculated separately, see section 6.2. Also the case of thermal emission from the HIFI oscillator window requires some explanation, see section 6.3.

6.2   Diffraction Calculations

6.2.1   Introduction

Three methods are used for the diffraction calculations

- method of stationary phase

- method with Fresnel-Integrals (after Born&Wolf).

- ASAP's coherent field synthesis

The coincidence of two or three methods gives confidence that the numerous radiometric multiplications with solid angles, areas of emitting/receiving surfaces etc. are correct.

The method of stationary phase is fairly general in application. The results are correct even for large angles of diffraction; very close (roughly < 1 degree) to the shadow limit the results tend to approach infinity and must be clipped.

The method with Fresnel-Integrals is restricted to simple cases (at least in the example worked out in Born&Wolf), therefore it is used only as a check in order to verify the results of the other two methods.

ASAP's coherent field synthesis may be applied for geometries where a coherent wavefront can be traced across the objects in question without disturbing the following field synthesis of ASAP. The method is less accurate, if large diffraction angles occur.

IRRADIANCE 57.28996 MM BEHIND A SCREEN WITH STRAIGHT EDGE

logENERGY
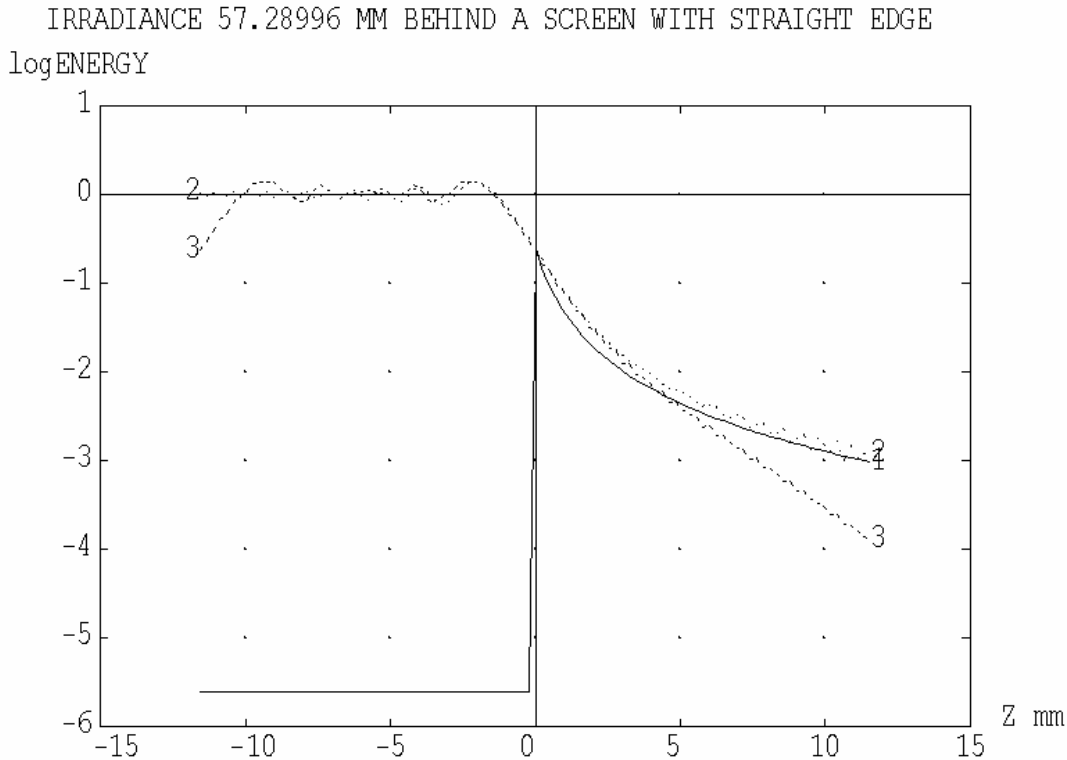
WAVELENGTH .1 MM. ABSCISSA: 1 MM = 1 DEGREE DIFFRACTION ANGLE.
CALCULATION DONE WITH: METHOD OF STATIONARY PHASE (CURVE 1),
FRESNEL INTEGRALS (CURVE 2), ASAP'S COHERENT FIELD SYNTHESIS (CURVE 3)

Fig. 6.2.1-1: Diffraction behind a straight edge calculated by three methods (wavelength is 0.1 mm).

These properties can be seen in fig. 6.2.1-1, i.e. a simple case selected only for the purpose of comparison. The irradiation impinging on a screen with straight edge is a plane wave (i.e. the source is at infinity). The intercepting plane is 57 mm behind the screen. On the left side there is the illuminated half while the shadow is on the right side. Near the shadow limit the linear dimension in mm coincides with 1 degree diffraction angle (it is proportional to the tangent of the diffraction angle). The logarithm(10) of the relative irradiance is plotted as obtained with the three methods. The line for the method of stationary phase has not been calculated in the illuminated region (therefore drops to quasi zero).

The cases treated in the next chapters are

- thermal emission from the gap between the cryocover and the surrounding baffle structure diffracted towards the field of view by instrument edges

- thermal emission from the gap of the sunshade diffracted into the field of view by the rim of the secondary mirror.

Both cases deal with gaps which have to be considered as high emissivity objects, thus are strong sources possibly causing appreciable diffraction effects.

The case with the secondary mirror as diffracting edge is a special case, since this diffracting edge can be seen by the detectors; it is imaged onto the rim of the cold stops / chopper elements probably without any appreciable clipping. Thus a single diffraction at the rim of the secondary is sufficient to redirect radiation onto the detectors. The case with the gap around the cryocover (and other similar cases) is different, at least another scattering/diffracting process is required before the diffracted rays enter the field of view. The reason for that is that all candidates for diffracting edges

- either cannot be seen by the detectors directly

- or are not irradiated by strong sources.

Doc. No: HP-2-ASED-TN-0023   Page: **38**
Issue: 2   of: **73**
Date: 21.10.02   File: HP-2-ASED-TN-0023_2.doc

6.2.2   Diffraction on the entrance of SPIRE with the cryocover gap as thermal source

It is known from the earlier analyses that the irradiation caused by purely specular paths diminishes within the experiments from element to element (starting at the experiment entrance). I.e. all thermally emitting objects (sunshade, conebaffle, etc.) generate rays with oblique incidence onto the experiments, these rays loose energy with each reflection at walls within the experiment. Thus near to the detector the irradiance is small while it is large near the entrance. Therefore diffraction at the entrance of SPIRE was chosen as example for the diffraction calculation.

The wavelength selected is 0.6 mm, i.e. the worst case for Herschel. The diffraction effect scales proportional to the wavelength.

As emitting element the gap between the cryocover and the surrounding baffle was chosen. The diffraction occurs at the entrance of SPIRE (see fig. 6.2.2-1). The intercepting plane for the diffracted rays and the incident rays is the SPIRE object thermal filter 1 at the telescope focal surface. Therefore this object is made absorbing in this calculation. In fig. 6.2.2-1 some incident rays are shown (more rays are used in the calculation). They are specularly reflected by the surfaces within the FP_UNIT, mainly by the walls, a reflectivity of 0.3 was assigned to these walls by RAL.

The diffracted rays were generated by the method of stationary phase at the right edge of the SPIRE entrance. They impinge directly onto the thermal filter 1, they are also redirected to it by reflection on the walls of the FP_UNIT, see fig. 6.2.2-2 (less rays shown than used in the calculation).

In fig. 6.2.2-3 the resulting relative irradiance onto the thermal filter 1 is shown with the lower curve for the diffracted rays. The upper curve in fig. 6.2.2-3 shows the irradiance of the purely specular rays impinging on the thermal filter 1, i.e. those rays redirected only by the walls of the SPIRE FP_UNIT. The purely specular rays yield a much larger irradiance than the diffracted ones. Therefore it is sufficient to perform further analyses of the propagation of the rays passing the thermal filter 1 with impinging specular rays only. It is not necessary to trace the diffracted rays further. Remind that the diffracted rays originate from a rim outside the direct view of the detector. Another scattering/diffracting process is necessary to redirect the rays to the path onto the detector.

There is another diffraction contribution from the opposite edge of the SPIRE input. This contribution is much smaller due to the larger diffraction angle. The edges at +Y and –Y of the SPIRE input yield a fairly small contribution due to their reduced length.

As consequence, the phenomenon of diffraction does not dominate in that case. There is a concurring specular path which dominates. This dominating purely specular path will be traced in subsequent analyses by investigation of the scattering effect by the thermal filter 1. Such a scattering directly opens the way towards the detector.

<div align="center">ERGÄNZEN !!!!!!!!!!!!!!!!!!</div>
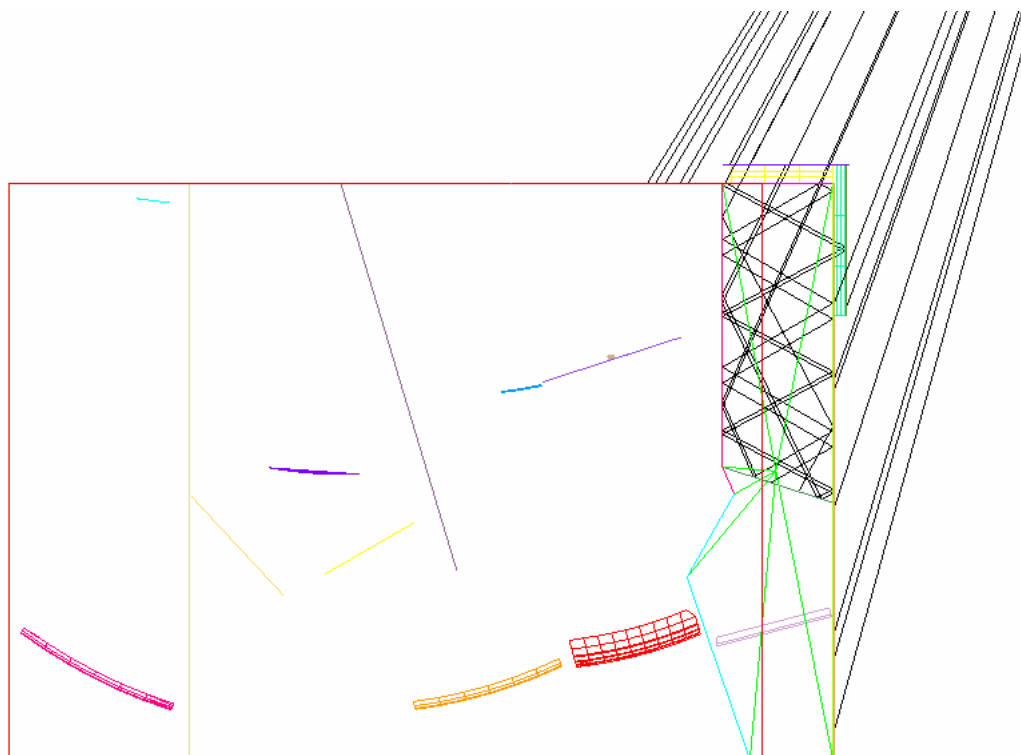
Fig. 6.2.2-1: Some incident specular rays from the cryocover gap

Unfortunately the scattering function of the thermal filter 1 is not known, so assumptions have to be made. Should RAL (in the future) state that a sharply-peaked Harvey scattering function be applicable, then the argument of the domination of the specular rays may be outweighed by the behaviour of that function. In that case the diffracted rays could also be used for a scattering calculation (in addition to the specular rays).
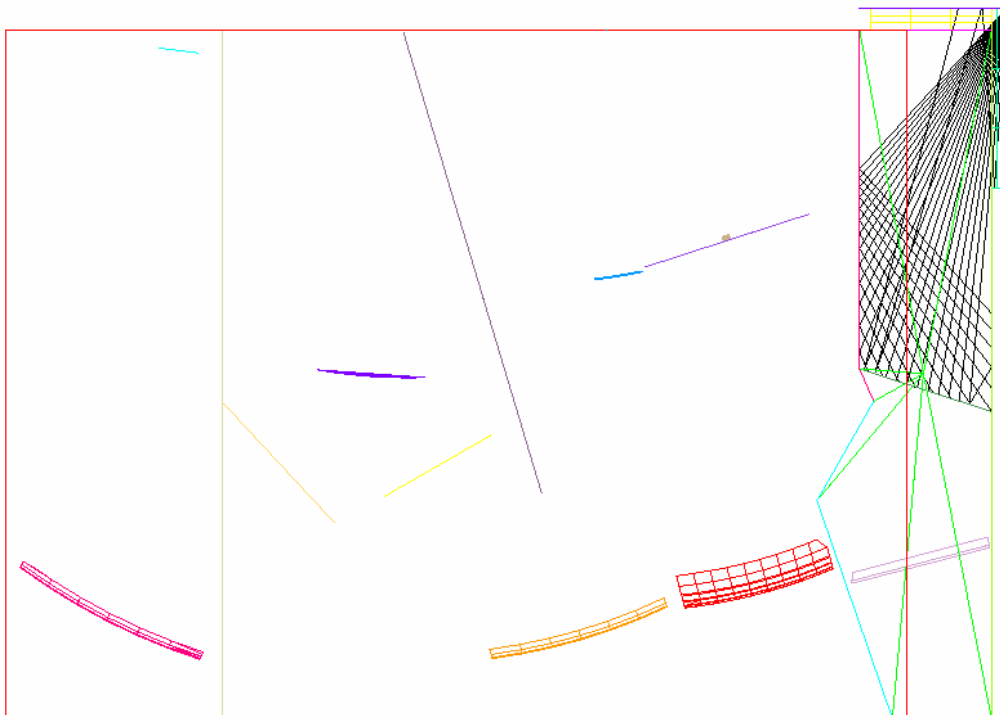
Fig. 6.2.2-2: Some rays diffracted at the right edge of the SPIRE input
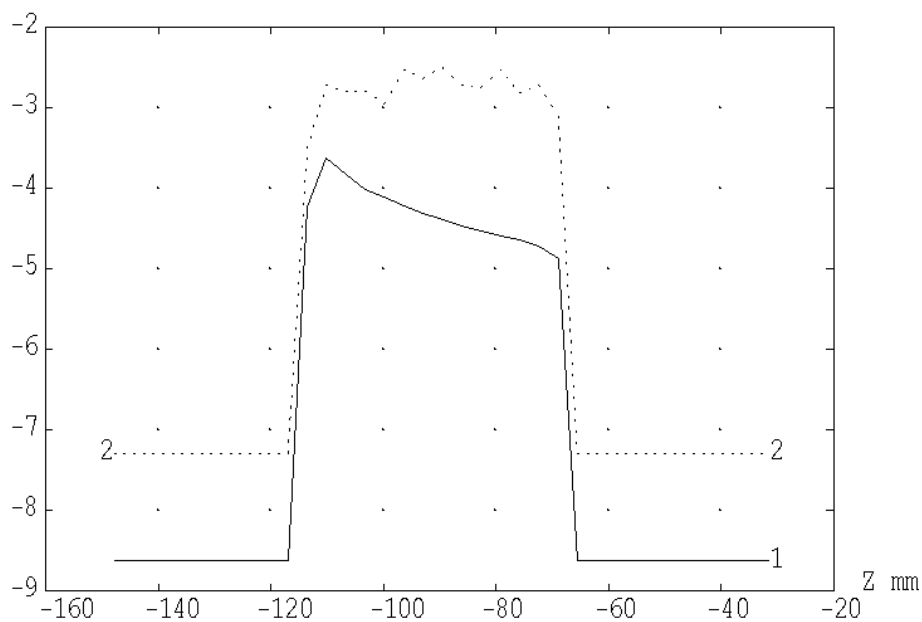
Fig. 6.2.2-3: Relative irradiance (logarithm(10)) onto the thermal filter 1 of SPIRE.
Lower curve: diffracted rays; upper curve: purely specular rays.

Doc. No: HP-2-ASED-TN-0023   Page: **41**
Issue: 2   of: **73**
Date: 21.10.02   File: HP-2-ASED-TN-0023_2.doc

The other diffracting edges within SPIRE are irradiated with diminishing irradiance when entering SPIRE further along the path towards the detector. So the diffraction effects diminish too.

The special case of the cold stop (the edge of which can be seen directly by the detector) was checked separately by a specular raytrace. There was a spurious ray with path

cryocover gap ---> CVV --> hexapod --> secondary mirror --> cold stop

with negligible flux. Thus it was verified that the cold stop edge is not irradiated directly by the cryocover gap with relevant irradiance.

The opening of PACS is irradiated with much less irradiance than SPIRE (< 2 %, mainly due to the lower entrance position of PACS and the position with +Z-coordinate resulting in a smaller view onto the cryocover). In addition, PACS uses smaller wavelengths than SPIRE. Therefore SPIRE is the worse case compared to PACS and for PACS the purely specular paths will dominate too (nevertheless scattering calculations will be described both for SPIRE and PACS in the next sections). The spurious ray with path

cryocover gap ---> CVV --> hexapod --> secondary mirror --> cold stop

with negligible flux exists for PACS too, no strong direct path onto the cold stop is present. Thus it was verified also for PACS that the cold stop is not irradiated directly by the cryocover gap with relevant irradiance.

We consider the calculations made above as representative for all edges not directly seen by the detectors, i.e. all edges in front of the cold stops of SPIRE and PACS (except for the case of the M2-assembly, see next section). There is confirmation from the experiment side that this is the case for all experiment edges in question

- for PACS by phone (Kayser-Threde)
- for SPIRE by documents.

Also the objects of the M1-baffle, heat shield 2 etc. obey that rule. So the next section describes the only relevant case for diffraction.

The only case known to have a somewhat small oversizing is the rim of the SPIRE thermal filter 1, there a minimum clearance of 1 mm occurs for some fraction of that rim. The rim of thermal filter 1 is imaged just outside the edge of the detector area, thus may affect only these edge array elements.

Remark: the cryocover gap used for these calculations was considered black during these calculations made in July 2002. Meanwhile this gap is closed nearly completely by high reflection elements. Therefore the tables on thermal self-emission does not contain any longer the black gap. Fig. 6.2.2-3 remains valid, since there a relative compsarison has been made which is not affected by the transition from high to low emissive elements.

6.2.3   Diffraction at the rim of the secondary mirror with the gap near the sunshade as thermal source

As mentioned already, the diffracting edge of M2 can be seen by the detectors; it is imaged onto the rim of the cold stops / chopper elements probably without any appreciable clipping. Thus a single diffraction at the rim of the secondary is sufficient to redirect radiation onto the detectors. Therefore a calculation of the diffracted radiation impinging on the telescope focal surface is sufficient for a judgement of that straylight case.

ASAP's coherent field synthesis was chosen for that calculation, since it is straightforward to include the two obscuring hexapod struts into the analysis (it would be quite laborious to do the same with the stationary phase method). 21 coherent point sources are placed along the gap, they radiate towards the rim of the secondary mirror. The beams are propagated onto the telescope focal surface. There the coherent field synthesis is done separately for each source. Afterwards the irradiance of each source is added incoherently. Fig. 6.2.3-1 gives an impression of the beams used for the calculation. The beams of two sources are clipped partially by two hexapod struts, so a possible diffraction effect by the struts is included. The experiment structure is not included, since the intention is to present a broader distribution of the diffracted radiation on the telescope focal surface in the graphs; the small experiment openings would include only a small fraction of the spatial distribution of the irradiance.

The radiance of the source is set to the same value as usual in our thermal calculations ($=1/\pi$ $1/(sr*mm^2)$), so a comparison with the radiation of the telescope mirrors can be done easily. The usual correction factors for emissivity ($=0.8$) and temperature (204 K) for the gap near the sunshade are applied. A normalization of the mirror contribution to 100% is included too. Thus the curves presented here are to be interpreted as in the earlier analysis: a value of 1.0 (or 0 in the log(10)-diagrams) corresponds to 1% of the thermal radiation of both telescope mirrors.

The irradiance is plotted across the Y-coordinate in fig. 6.2.3-2, across the Z-coordinate in fig. 6.2.3-3. The positions of PACS and SPIRE are near Z=+80 and Z=-90 mm. Both diagrams are valid for a wavelength of 0.2 mm thus touch both wavelength regions of PACS and SPIRE. The corresponding figs. 6.2.3-4 and 6.2.3-5 are valid for 0.67 mm wavelength (SPIRE only). The positions of the scans can be seen in the figure subscripts.

The irradiance for PACS at 0.2 mm wavelength is near 3....5% of the thermal radiation from the mirrors. The figures indicate for SPIRE that the straylight contribution is between 20.....40% (0.2 mm...0.67 mmm) . One should take into account that the rim of the secondary is seen with reduced sensitivity due to the edge taper of 8 dB (or 13%) introduced by the horns of SPIRE (the edge taper is not included in the figures which represent the pure diffraction variation). So the straylight for SPIRE is reduced to about 3....6% (5% will be inserted in the summarizing tables).

The scaling law for diffraction (proportional to wavelength) is not the only parameter influencing the diffraction curves; due to the comparison with the thermal radiation of the telescope mirrors also the variation of the Planck curves with wavelength for different temperatures counts.
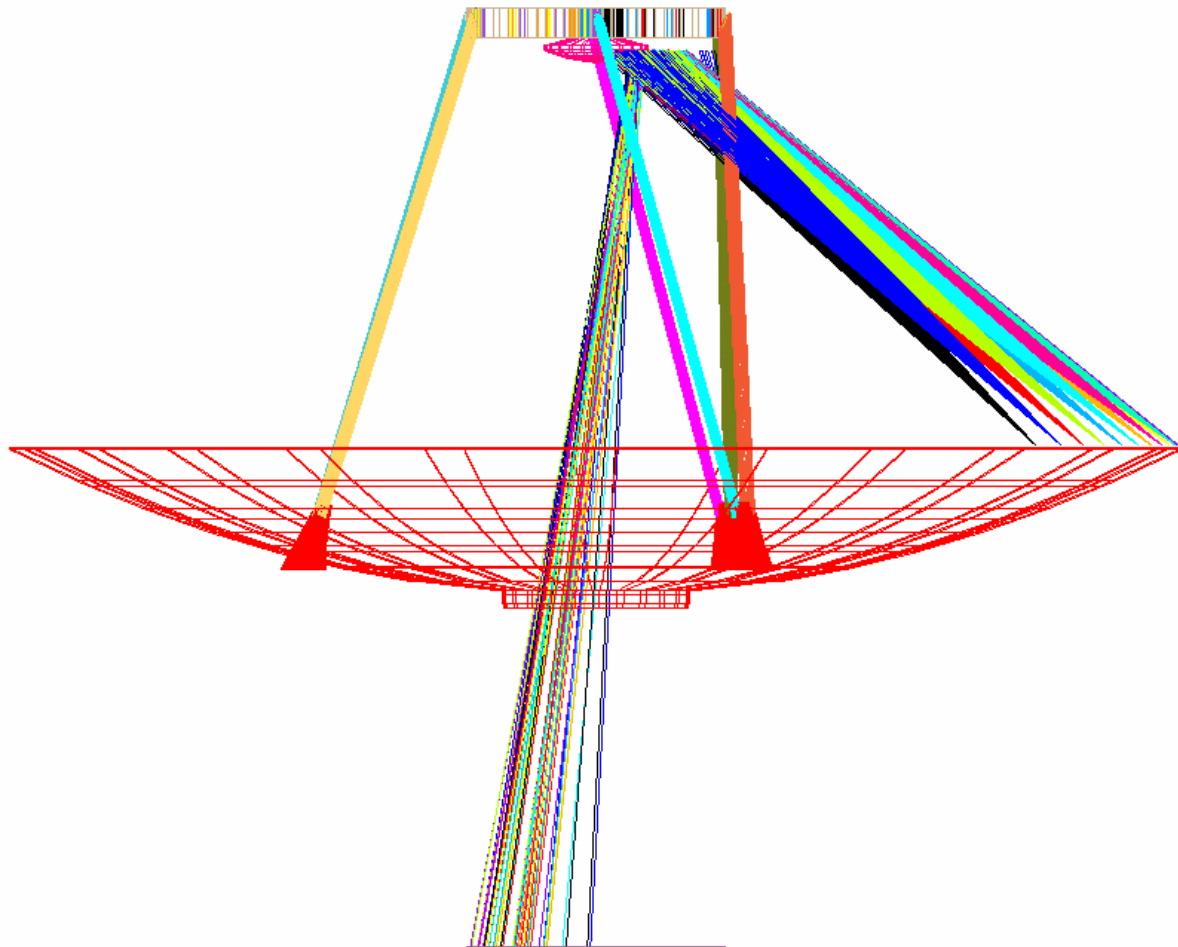
Fig. 6.2.3-1: Beams used for the calculation of diffraction at the rim of the secondary mirror, source is the gap near the sunshade.

All these numbers describe a worst case situation with the average temperature of the sunshade set at 204 K, i.e. the thermal hot case. Nevertheless, other thermal contributions come on top of the percentages mentioned. So mechanical changes improving the situation are highly desirable, e.g. the introduction of a small reflecting element within the gap. Presently the gap has an area of 9000 cm^2 with high emissivity.

log FLUX / sq-MM

COORDINATE IN SYSTEM FOCUS
CONTINUOUS LINE THROUGH CENTER OF SYSTEM FOCUS
DOTTED LINES AT DISTANCE Z=+-89.53596 MM FROM CENTER OF SYSTEM_FOCUS
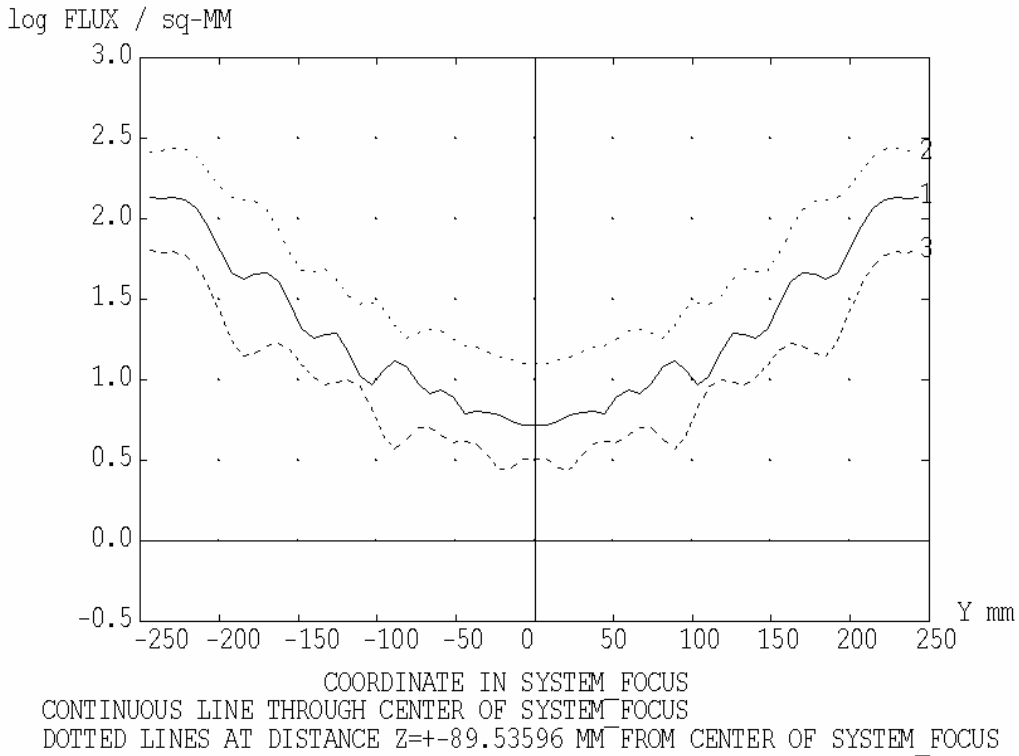
Fig. 6.2.3-2: Irradiance on system focal plane with scans across Y-coordinate (wavelength 0.2 mm)

log FLUX / sq-MM

COORDINATE IN SYSTEM FOCUS
CONTINUOUS LINE THROUGH CENTER OF SYSTEM FOCUS
DOTTED LINES AT DISTANCE Y=+-24.8711 MM FROM CENTER OF SYSTEM_FOCUS
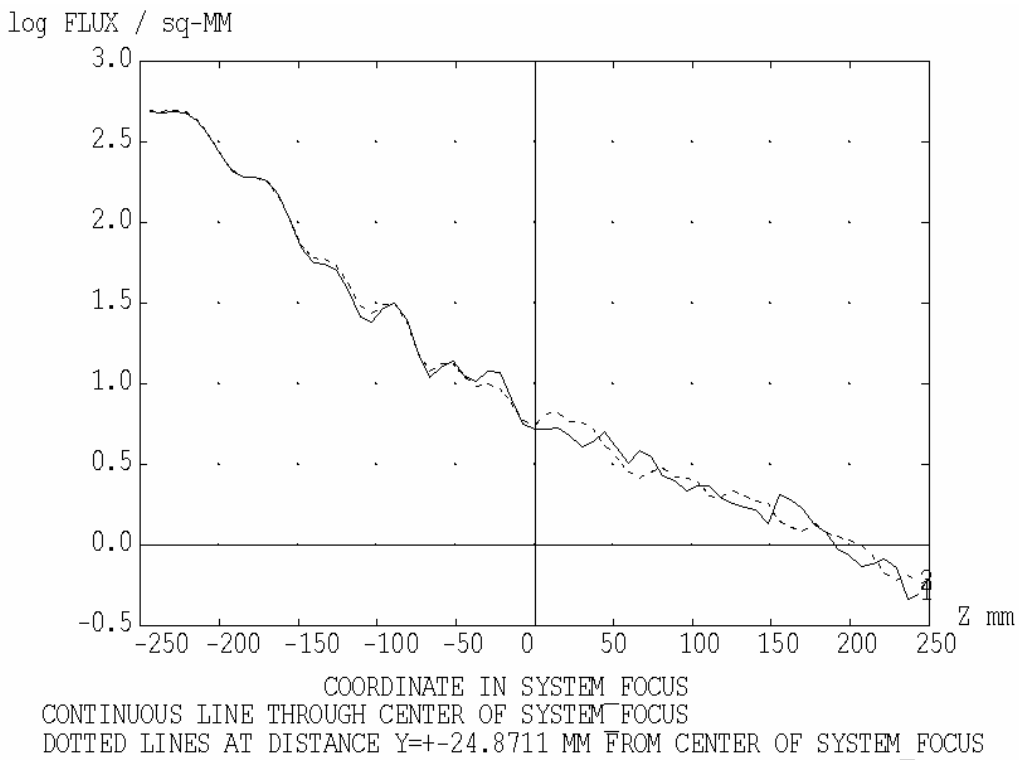
Fig. 6.2.3-3: Irradiance on system focal plane with scans across Z-coordinate (wavelength 0.2 mm)

log FLUX / sq-MM

COORDINATE IN SYSTEM_FOCUS
CONTINUOUS LINE THROUGH CENTER OF SYSTEM_FOCUS
DOTTED LINES AT DISTANCE Z=+-89.53596 MM FROM CENTER OF SYSTEM_FOCUS
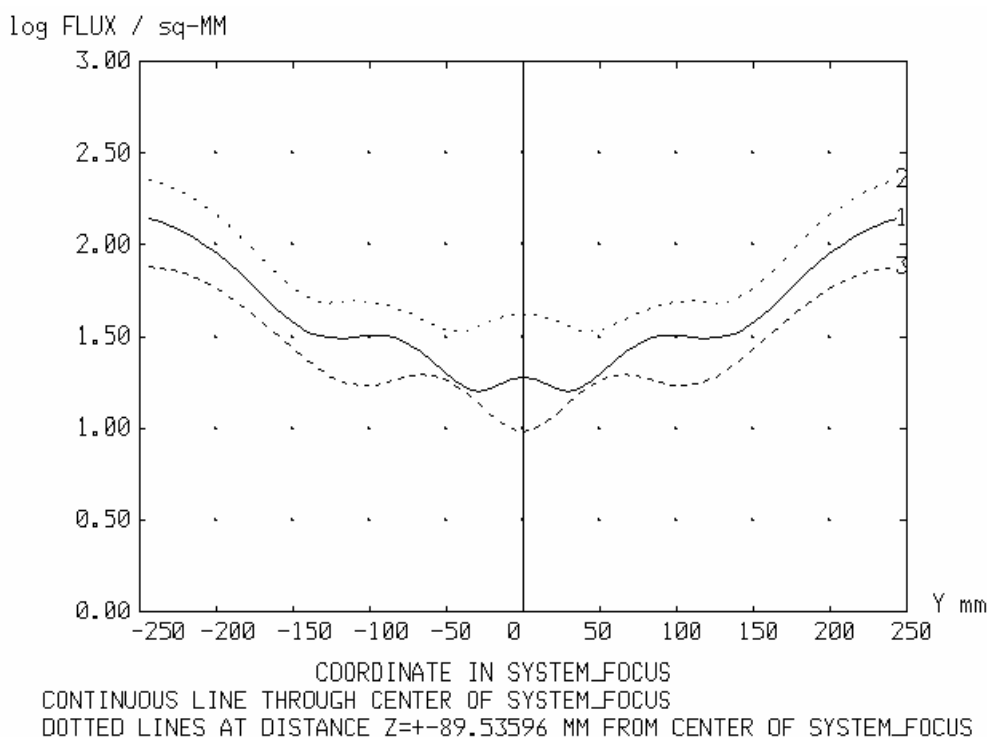
Fig. 6.2.3-4: Irradiance on system focal plane with scans across Y-coordinate (wavelength 0.67 mm)

log FLUX / sq-MM

COORDINATE IN SYSTEM_FOCUS
CONTINUOUS LINE THROUGH CENTER OF SYSTEM_FOCUS
DOTTED LINES AT DISTANCE Y=+-24.8711 MM FROM CENTER OF SYSTEM_FOCUS

Fig. 6.2.3-5: Irradiance on system focal plane with scans across Z-coordinate (wavelength 0.67 mm)

As mentioned, a complete comparison with the method of stationary phase was not programmed due to the complexity with the hexapod struts and the distribution of sources along the gap. Neverthe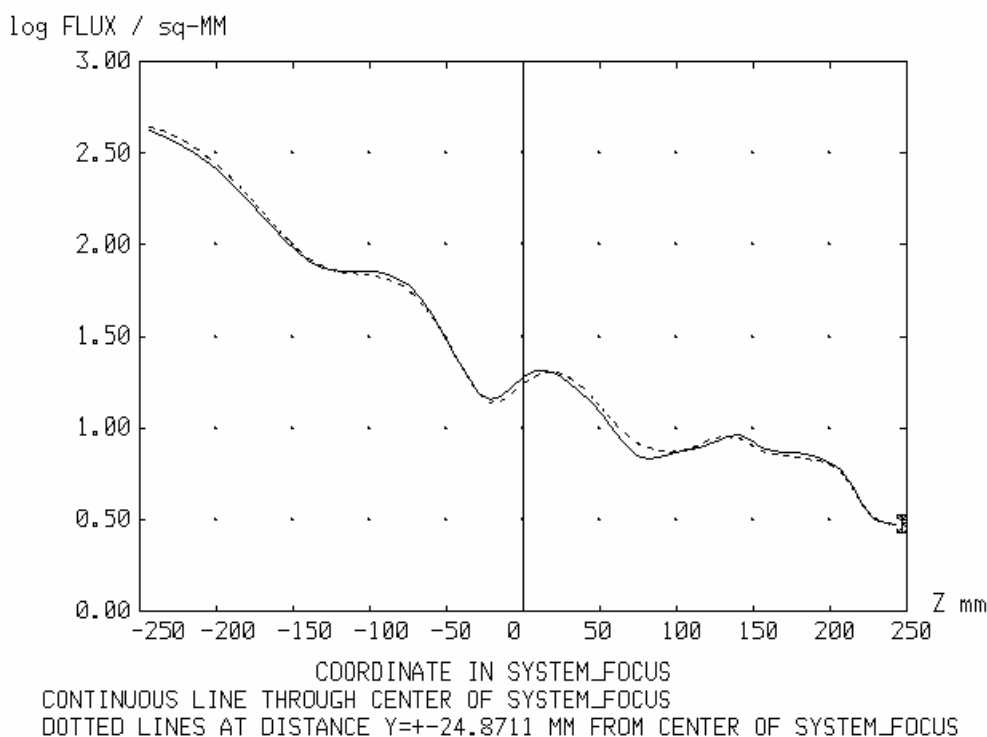less, a partial comparison has been worked out by setting only a single source in the gap at Y=0. For that case (which does not represent the complete radiometric situation) a relative comparison has been programmed with the method of stationary phase. A scan across Z-coordinate at Y=0 in the telescope focal surface is the result shown in figs. 6.2.3-6 (wavelength 0.2 mm) and 3-7 (wavelength 0.67 mm). The method of stationary phase (as applied) does not contain such a refinement in its mathematics that fringes could appear; however, the overall comparison is acceptable. At the shadow limit the curve for the stationary phase tends to infinity, therefore it has been clipped as usual (at the position of the dip which is not real).

The comparison shows that ASAP's coherent field synthesis is acceptable for the case of diffraction at the rim of the secondary of a source nearby the nominal beam. The fringes seen in figs. 6.2.3-6 and 6.2.3-7 are less salient in the preceeding figures, since there an incoherent superposition of several coherent sources along the gap has been calculated. The results of the coherent calculation are somewhat dependent on the input parameters (number of rays etc.), thus the accuracy of the results certainly has to be considered with caution, we think it is not better than a factor of 3...5. ASAP's coherent field synthesis obviously is approaching its limits for such calculations.

The wavelength 0.08 mm (the short wavelength limit of PACS) is not within the cases presented here. At this wavelength, ASAP's coherent field synthesis partially encountered the so-called 'departures from paraxial approximation', i.e. an ASAP warning that the synthesis may not be correct. The straylight contribution for PACS at 0.08 mm will be nearly identical to 0.2 mm, since the influences of

- the wavelength dependence of the diffraction
- the wavelength dependence of the Planck curve

nearly cancel out when changing wavelength from 0.2 mm to 0.08 mm.

log FLUX / sq-MM

COORDINATE IN SYSTEM FOCUS
CONTINUOUS LINE IS ASAP'S COHERENT FIELD SYNTHESIS
DOTTED LINE IS METHOD OF STATIONARY PHASE

Fig. 6.2.3-6: Relative comparison of two methods with a single source in the gap diffracted at the rim of the secondary mirror, wavelength = 0.2 mm

log FLUX / sq-MM

COORDINATE IN SYSTEM FOCUS
CONTINUOUS LINE IS ASAP'S COHERENT FIELD SYNTHESIS
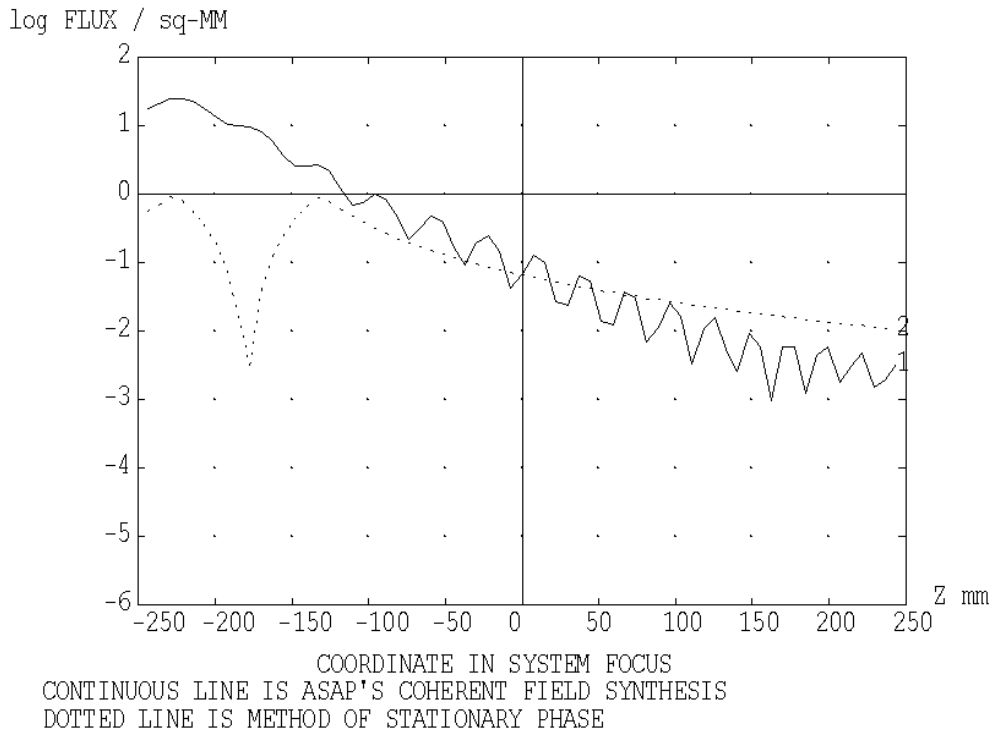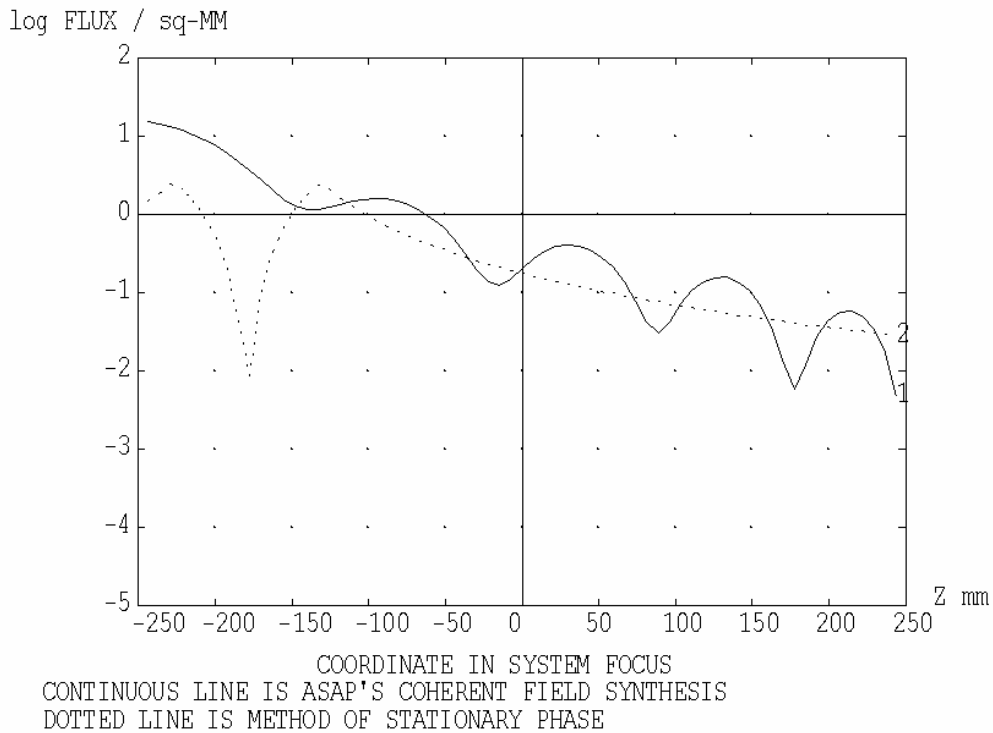DOTTED LINE IS METHOD OF STATIONARY PHASE

Fig. 6.2.3-7: Relative comparison of two methods with a single source in the gap diffracted at the rim of the secondary mirror, wavelength = 0.67 mm

6.3   Thermal Emission from the HIFI Oscillator Window

The windows for feeding the oscillator radiation into the cold instrument region also feed in thermal radiation. We assume a black thermal radiation of temperature 150 K there with no restriction of the solid angle (i.e. hemispherical). The ASAP HIFI model contains mirrors and housing walls. The walls are quoted to have a reflectivity similar to that of mirrors, so we adopt a reflectivity of 0.99. Both the mirrors and the walls transport the thermal radiation towards the internal opening of HIFI, i.e. towards HIFI mirror M3, from there the radiation aims at +X-direction.

A first trial with a lambertian emitter at the oscillator window position with the PACS and SPIRE detectors as receiving surfaces fails, the large number of zigzag reflections within HIFI did not lead to reasonable results. Therefore the whole path was split into several steps

     a)   transmission of thermal radiation through the HIFI compartments (stepwise)

     b)   radiation onto PACS and SPIRE (via the M2-assembly) from a fictive thermal emitter at the HIFI opening near M3.

Step b) is described first. The black thermal radiation of temperature 150 K assumed at the oscillator window is placed at the HIFI opening near M3, the resulting radiation (via the M2-assembly) towards PACS and SPIRE clearly represents a worst case. The numbers found are 4.2% (PACS) and 5.3% (SPIRE) (with 100% as contribution of the telescope reflectors). They are not negligible, therefore it is necessary to calculate step a) too.

The transmission of thermal radiation through the HIFI compartments is calculated for
- compartment 1
- compartment 1 plus 2.

the compartment numbering is shown in fig. 6.3-1.

The transmission calculations start with lambertian sources at the LOU window, the transmission is evaluated as the ratio of the fluxes out/in. The results are

Compartment	Transmission
1	0.3
1+2	0.09

The numbers depend strongly on the assumed wall reflection assumed to be 0.99.

There are 5 compartments, the table above indicates that each compartment yields a transmission with factor 0.3, 5 compartments could give 0.3^5=0.0024. Although only compartments 1 and 2 have been calculated, it is safe to state that the total transmission for all compartments is smaller than 0.01. So the numbers of worst case of step b) now reduces to <0.04% (PACS) and <0.05% (SPIRE). These numbers are small enough for the statement that the thermal radiation from the HIFI oscillator does not play an important role.

Compartments: **2**   **5**   **towards M2** ↑

Compartments: **1**   **3**   **4**   **M3** ↑
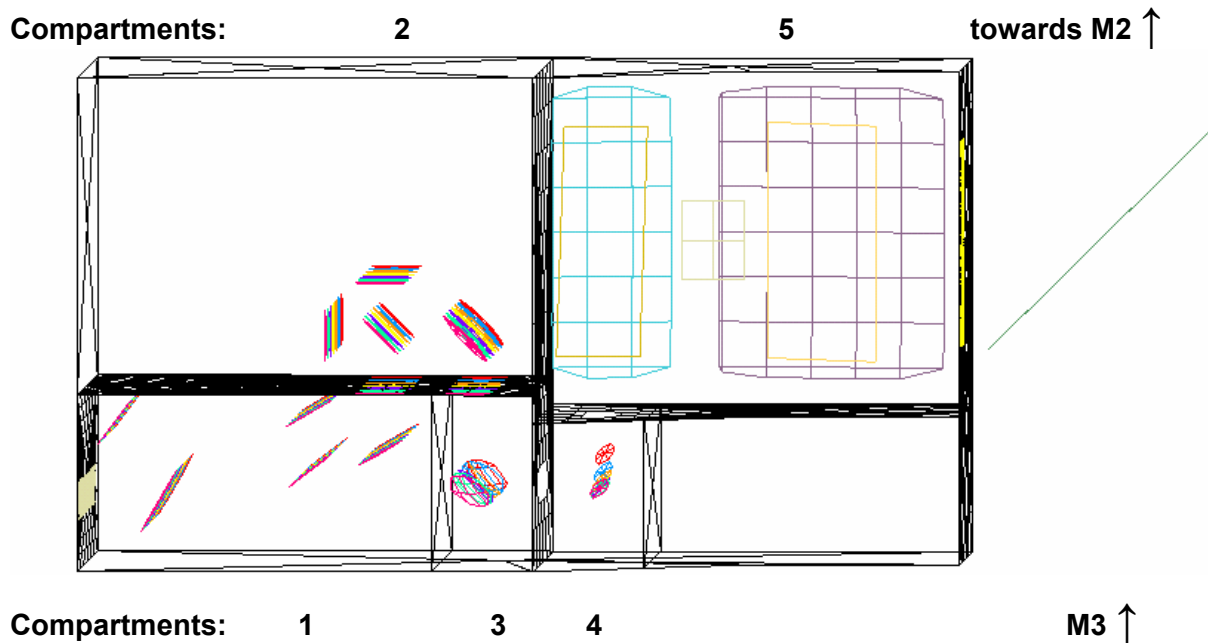
Figure 6.3-1   ASAP-HIFI model with compartment numbering. The numbers increase from the local oscillator windows (lower left side) to the inner opening towards M3 and M2 (telescope secondary mirror).

6.4   Results

Since the requirement on self emission is a number relative to the self emission of the reflectors, all calculations are done without use of a unit for flux (e.g. Watt). The emitting raygrids within ASAP all have an emitting radiance of $1/\pi$ per mm^2 per steradian. The raytrace yields a total flux value for the SPIRE/PACS detectors. The flux onto the detectors from a specific object (e.g. the sunshade) is divided by the sum of fluxes calculated for M1 and M2.

This relative flux for the specific object has to be corrected with two factors:

- Temperature correction factor: thermal emission of emitting object temperature divided by thermal emission of a 70 K object (temperature for M1 and M2). This temperature correction factor depends on the wavelength. The wavelength choice was made such that the worst case is selected, i.e.

  o 80 μ (PACS), 230 μ (SPIRE) for emitting objects warmer than the telescope reflectors.

  o 230 μ (PACS), 670 μ (SPIRE) for colder objects.

- Emissivity correction factor: emissivity of object versus emissivity of M1 and M2.

The results are values averaged over the respective detector area.

The contribution of M1 + M2 has been set to 100 so:

- the violation of the 10% thermal emission requirement occurs if the numbers exceed 10.

The table 6.4-1 gives an overview on the expected worst case situation for the case with the large scattercone, table 6.4-2 treats the case of the small scattercone. The expected temperatures of the CVV and the surrounding objects are about 75 K in the worst case, if the telescope itself is at 70 K.

For most of the emitting objects, the purely specular paths are the dominant ones. However, some paths do not follow this rule, they are marked with

- Sc = scattering, the object indication where scattering takes place is added

- D = diffraction, the object indication where diffraction takes place is added.

The only diffraction path is that from the gap near the sunshade.

For the other lines, it is indicated whether the contribution is only specular or only scattered. If nothing is indicated, then it is the sum of specular and scattered.

Table 6.4-1:   Self emission onto pacs/spire detectors for large scatter cone

emitting object	temperature/ emissivity	scattering(Sc)/ diffraction(D) on	PACS detector	SPIRE detector
sunshade	204 K / 0.05	Sc: M1/M2, +spec.	1.545	0.295
gap between sunshade and M1	204 K / 0.90	only Sc: M1 / M2	1.473	0.624
gap between sunshade and M1	204 K / 0.90	only D: M2(rim)	4.0	5.0
Hexapod of telescope (from RD1)			4.17	4.17
M1+M2 (from RD1)			9.85	9.85
scattercone (from RD1)			3.09	3.09
annular M2 surface as difference betw. large and small scatter cone			0	0
M1-baffle flat	75 K / 0.05		0.585	0.042
M1-baffle cone / cylinder.	75 K / 0.05		1.602	0.065
gap betw. M1-baffle cone and cyl.	75 K / 0.90		0.240	0.010
reflecting cryocover	75 K / 0.05		0.585	0.101
black cryocover	75 K / 0.80	only specular	9.342	0.254
black cryocover	75 K / 0.80	only Sc: M2	0.013	0.018
black cryocover	75 K / 0.80	only Sc: experim.	0.001	1.341
reflecting objects near cryocover	75 K / 0.05		0.010	0.023
CVV top	75 K / 0.05		0.078	0.040
gap betw. CVV and heat shield 2	60K / 0.90		0.207	0.520
heat shield 2 black	43 K / 0.80	only specular	1.967	0.182
heat shield 2 black	43 K / 0.80	only Sc: experim.	0.099	3.817
instrument shield (tube only)	12 K / 0.80		0.002	0.027
LOU window	150 K / 0.90		0.05	0.04
sum with black cryocover			38.324	29.408
sum with reflecting cryocover			29.553	27.896
sum with reflecting cryocover and with reflecting gap between sunshade and M1			24.384	22.584

Table 6.4-2:   Self emission onto pacs / spire detectors for small scattercone

emitting object	temperature/ emissivity	scattering(Sc)/ diffraction(D) on	PACS detector	SPIRE detector
sunshade	204 K / 0.05	Sc: M1/M2, +spec.	1.596	0.319
gap between sunshade and M1	204 K / 0.90	only Sc: M1 / M2	1.477	0.609
gap between sunshade and M1	204 K / 0.90	only D: M2(rim)	4.0	5.0
Hexapod of telescope (from RD1)			4.34	4.34
M1+M2 (from RD1)			7.54	7.54
scattercone (from RD1)			0.62	0.62
annular M2 surface as difference betw. large and small scatter cone			2.47	2.47
M1-baffle flat	75 K / 0.05		1.801	0.911
M1-baffle cone / cylinder.	75 K / 0.05		4.245	0.092
gap betw. M1-baffle cone and cyl.	75 K / 0.90		0.637	0.014
reflecting cryocover	75 K / 0.05		1.044	0.098
black cryocover	75 K / 0.80	only specular	16.688	0.243
black cryocover	75 K / 0.80	only Sc: M2	0.013	0.018
black cryocover	75 K / 0.80	only Sc: experim.	0.001	1.300
reflecting objects near cryocover	75 K / 0.05		0.411	0.230
CVV top	75 K / 0.05		0.244	0.004
gap betw. CVV and heat shield 2	60K / 0.90		0.218	0.484
heat shield 2 black	43 K / 0.80	only specular	2.082	0.024
heat shield 2 black	43 K / 0.80	only Sc: experim.	0.098	3.699
instrument shield (tube only)	12 K / 0.80		0.002	0.027
LOU window	150 K / 0.90		0.05	0.04
sum with black cryocover			48.533	27.984
sum with reflecting cryocover			32.875	26.521
sum with reflecting cryocover and with reflecting gap between sunshade and M1			27.702	21.223

the lines 'instrument shield' and 'LOU window' have been copied from case large scattercone

There are three major positions in the tables which cause an increase compared to issue 1:

- the diffraction at the rim of M2 with the sunshade gap as source (not calculated for issue 1)

- the contribution for M1+M2 (from RD1, specular paths across hexapod structure etc.)

- the black version of the cryocover (only reflecting in issue 1).

As done for issue 1, several sums are listed (without specific emitters) in order to ease the copmparison.

Comparison SPIRE-PACS

Some differences between SPIRE and PACS are due to their different location in the focal region of the telescope. But more important is the fact that the ASAP model of SPIRE has a closer limitation of the SPIRE beam to the boundary of M2 than is the case for PACS (noticeable in figures 4.2-4 and 4.2-5). Whether this limitation in reality will be as close as in the ASAP model, depends on problems of misalignment etc.. Thus the values for SPIRE in some cases could come closer to those of PACS in case of misalignment. Nevertheless, some differences will always be present due to the apodization across the pupil realized by SPIRE.

Comparison large /small scattercone

The largest difference in the values between both scattercones exists for the black cryocover as emitting object. The dominating path for the case of the small scattercone is illustrated in figure 6.4-1.
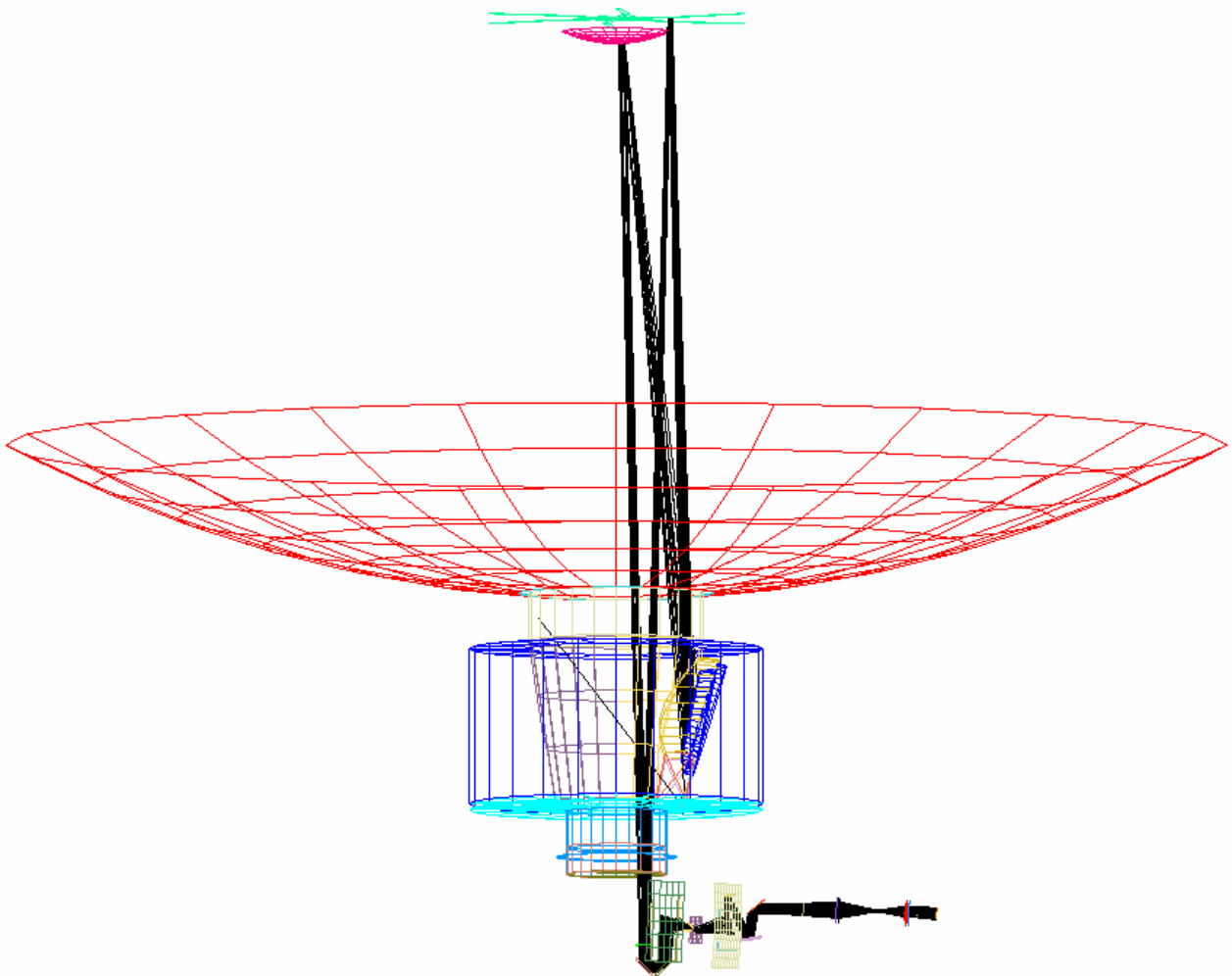
Figure 6.4-1: Path from the cryocover via M2 and hexapod bar towards PACS (detail below)
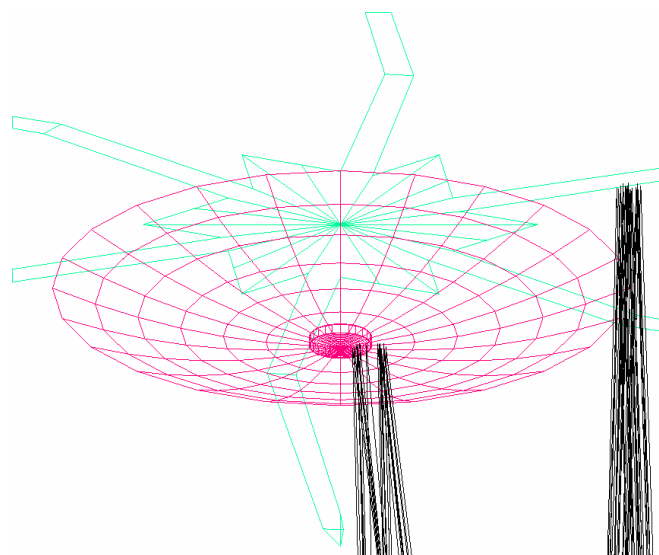
Marginal paths

Many paths found are 'marginal' paths, they involve small solid angles within the path, i.e. a small angular redirection of the rays is sufficient for a blockage of that path. An example is shown in figure 6.4-2 dealing with the mentioned beam limitation on the pupil, i.e. M2. It is clear that the values for the marginal paths have to be considered with caution, since usually only few rays find their way to the detectors due to the small solid angles. Some of these paths are marginal only in terms of solid angle, but not in terms of flux.

Figure 6.4-2: Marginal path involving the small solid angle of visibility of the hexapod bar surface to the PACS detector.

Annular M2-difference surface

The scattercone is treated as a thermal straylight source and quoted with values from RD1. Large and small scattercone exhibit thermal self emission proportional to the area. Therefore the small scattercone apparently is favourable at first sight. However, the small scattercone is surrounded by M2-surface up to the radius of the large scattercone, this a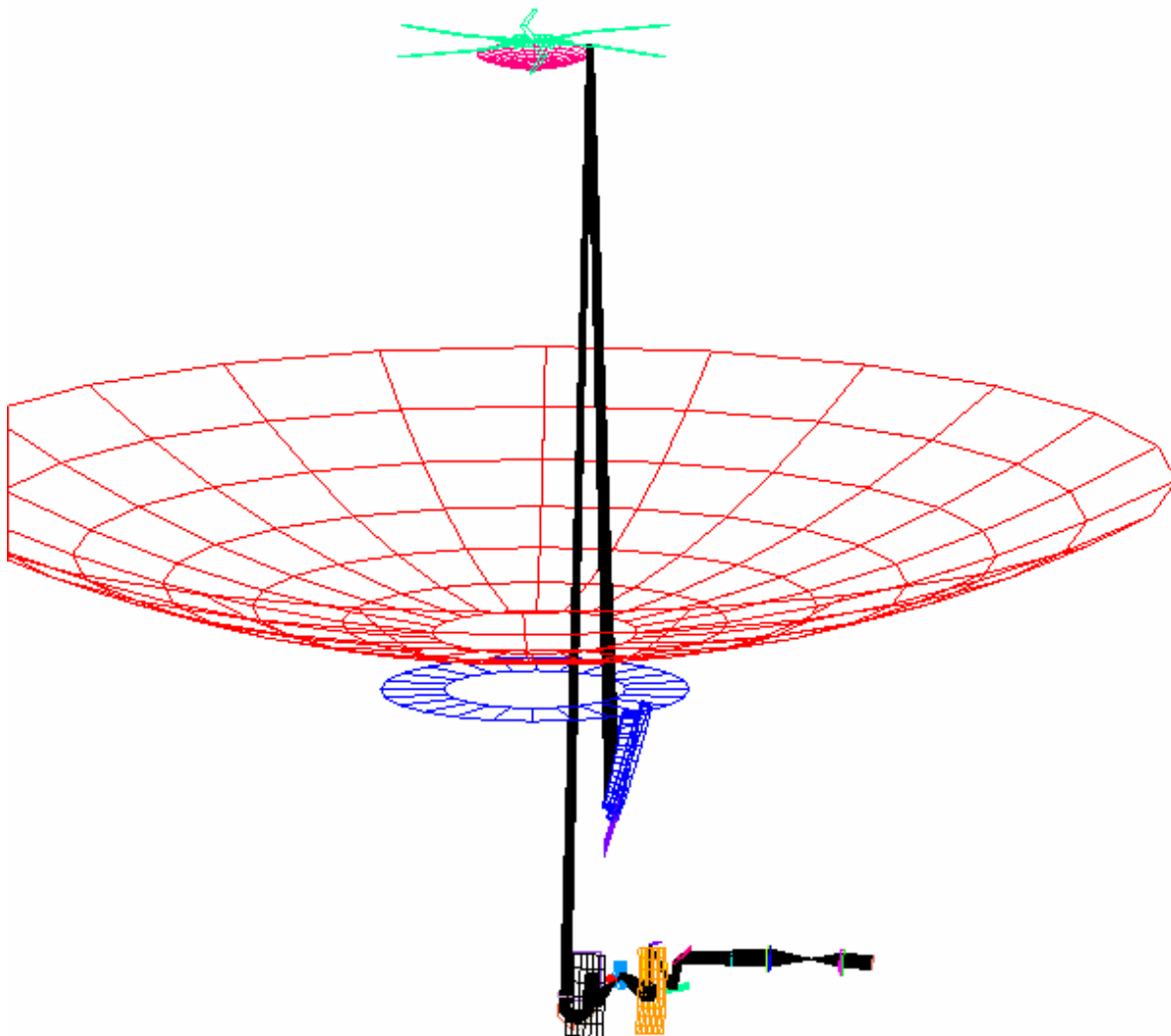nnular M2-surface also adds to the thermal irradiation of the experiments. Therefore we added a line representing the thermal contribution of this annular M2-surface with

- zero contribution in the case of the large scattercone

- the difference contribution of the annular M2-surface for the case of the small scattercone,

so that the comparison between small and large scattercone is more realistic. A suggestion in that direction came from SRON, we adopt this suggestion.

Sunshade

The contributions from the sunshade have an additional path (compared to the situation of issue 1), it is the chamfer on the outer rim of M2, no chamfer was present in the model for issue 1. If this chamfer is not as regular as it is simulated in the present ASAP model, then this path will be reduced. Presently this path contributes 70% of the value for PACS for the line 'sunshade' (less for SPIRE).

Gaps

The gap between sunshade and the outer rim of mirror M1 should be closed too as the numbers show, therefore a sum without this gap is listed too. Gap closure has been initiated, but no details have been fixed yet.

Another gap (existing in issue 1) was removed due to design improvement, i.e. the gap between the inner rim of mirror M1 and the M1-baffle.

Two gaps actually have not been calculated by a dedicated ASAP run, but the values have been deduced by similarity of stray paths to the neighbouring objects (with appropriate emissivity/temperature correction if applicable):

- the gap between cylindrical/conical parts of the M1-baffle (similarity to that parts)

- the gap between the CVV and heat shield 2 parts (similarity to heat shield 2.)

Reflecting objects near cryocover

They correspond to the inner cavity objects in issue 1. There they were treated as apparent high emissive surfaces, now they have been replaced by objects reflecting the design improvement, i.e. mechanical elements closing nearly all gaps around the cryocover. Therefore a low emissivity is used here.

Scattering within experiments

For most cases scattering within the experimants is negligible. The exceptions from that rule are two extended black surfaces irradiating SPIRE:

- the black cryocover

- the black heat shield 2.

It is important to note the assumptions on the scattering function of thermal filter 1 of SPIRE described in section 4.2. There is no information available on the corresponding scattering function.

Reductions for some worst case situations

Several paths exist for which the present model and the standard ASAP trace procedure yields worst case results. Two cases are important.

The elliptical struts of the telescope are approximated with a polygonal cross section with 24 sides. Therefore slim plane surfaces exist in the model whereas the in reality there will be a curved surface. The polygonal modelling has the advantage to highlight paths which might be overlooked with curved surfaces (due to insufficient ray statistics), thus is very helpful as a first step. However these paths could be overestimated. As an indication of the possible straylight reduction we tentatively multiply the paths involving the struts by a factor of 0.2; however, this factor is purely fictive. A (possibly iterative) calculation is planned for these paths, this refinement of the calculations shall produce (hopefully) more realistic straylight values.

The other important case for improvements deals with the reflections from the lower plane surface of the hexapod bars. These bar surfaces can be seen by the experiments

- either directly (but with small solid angle) just besides the rim of M2

- after reflection on M2 and M1.

The last path is under investigation by SRON w.r.t. reflection producing standing waves for HIFI, rounding or tilting of the lower bar surfaces are in discussion as improvement. Tilting may reduce some straylight paths, but could open others. So rounding may be the selected remedy. In order to give an indication what could be gained by a rounding, we introduce tentative reduction factors

- 0.5 for the direct view just besides the rim of M2

- 0.2 for the paths across M2 and M1.

As an indication of the possible straylight reduction we present table 6.4-3 (large scatter cone only) where the paths involving the struts or the hexapod have been tentatively multipied by reduction factors explained above. Table 6.4-3 has to be compared with table 6.4-1.

It is not known whether there exist possibilities of improvement for reduction of the 10% contribution from M1+M2 (cited from RD1).

Summary for thermal self emission

The requirement of 10% is violated. The worst case situation is the small scattercone with a black cryocover resulting in 50% for PACS. For the large scattercone the numbers differ between 21% and 38% depending on how much improvement (sunshade gap) is possible and on the decision on the cryocover emissivity. Straylight aspects yield the following recommendations

• large scattercone

• reflecting cryocover

• round hexpod bar surfaces

but it is known that ground testing arguments may overrule the straylight argument in favour of the reflecting cryocover. The disadvantages of the large scattercone are described in section 5 (obscuration and resolution).

Table 6.4-3:   Self emission onto pacs and spire detector for large scattercone. reduced
contributions from rounded hexapod bar surface and struts.

emitting object	temperature/ emissivity	scattering(Sc)/ diffraction(D) on	PACS detector	SPIRE detector
sunshade	204 K / 0.05	Sc: M1/M2, +spec.	1.545	0.295
gap between sunshade and M1	204 K / 0.90	only Sc: M1 / M2	1.473	0.624
gap between sunshade and M1	204 K / 0.90	only D: M2(rim)	4.0	5.0
hexapod of telescope (from RD1)			4.17	4.17
M1+M2 (from RD1)			9.85	9.85
scattercone (from RD1)			3.09	3.09
annular M2 surface as difference betw. large and small scatter cone			0	0
M1-baffle flat	75 K / 0.05		0.302	0.016
M1-baffle cone / cylinder.	75 K / 0.05		0.750	0.040
gap betw. M1-baffle cone and cyl.	75 K / 0.90		0.1125	0.006
reflecting cryocover	75 K / 0.05		0.28	0.088
black cryocover	75 K / 0.80	only specular	4.465	0.051
black cryocover	75 K / 0.80	only Sc: M2	0.013	0.018
black cryocover	75 K / 0.80	only Sc: experim.	0.001	1.341
reflecting objects near cryocover	75 K / 0.05		0.002	0.005
CVV top	75 K / 0.05		0.018	0.012
gap betw. CVV and heat shield 2	60K / 0.90		0.078	0.385
heat shield 2 black	43 K / 0.80	only specular	0.685	0.036
heat shield 2 black	43 K / 0.80	only Sc: experim.	0.099	3.817
instrument shield (tube only)	12 K / 0.80		0	0.005
LOU window	150 K / 0.90		0.05	0.04
sum with black cryocover			30.703	28.801
sum with reflecting cryocover			26.505	27.479
sum with reflecting cryocover and with reflecting gap between sunshade and M1			21.336	22.168

7   Sources outside the FOV (Earth, Moon)

7.1   Specular paths from Moon and Earth

The specular paths from moon/earth found during the calculations for issue 1 led to the recommendation of rounding the struts of the hexapod assembly. As already mentioned, the elliptical struts of the telescope are approximated with a polygonal cross section with 24 sides. Therefore slim plane surfaces exist in the model whereas the reality will be a curved surface. The polygonal modelling has the advantage to highlight paths which might be overlooked with curved surfaces (due to insufficient ray statistics), thus is very helpful as a first step. However these paths could be overestimated. A (possibly iterative) calculation is planned for the paths across the elliptical struts, this is reserved for the next issue no. 3

Therefore the calculations described here are those of issue 1 (unchanged), i.e. those with a rectangular cross section.

There are some specific directions from which the Moon or the Earth can be reflected specularly via various Hexapod structures into the instrument detectors. Most of these directions (except two smaller ones, which have not been analysed yet) are close to the limit for the possible moon directions, at around 20 degrees from the X-axis; therefore they are affected by the Moon (and bright stars) only and not by the Earth.

Figure 7.1-1 shows these directions for the case of the SPIRE detector, gained by a backward trace.

Figure 7.1-2 shows these directions for the case of the PACS detector, gained by a backward trace.

Two of the most important paths for SPIRE are shown in figure 7.1-3 and figure 7.1-4

Figure 7.1-1: Directions from which specularly reflected rays can hit the SPIRE detector.

Plot of directions towards the sky. The center of this polar diagram is the +Z axis. The circles around the +Z axis have distances of 10 degrees.

The outermost line roughly represents the limiting direction for the moon.

The limit for the earth is between the 2nd and the 3rd circle from outside.

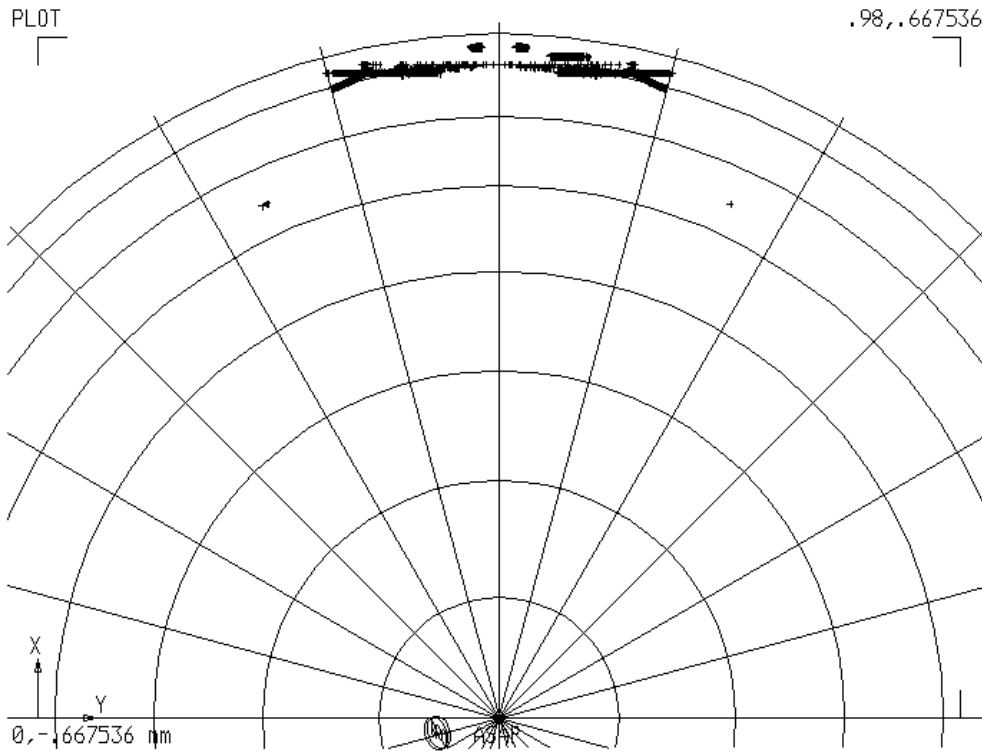Each + sign represents a direction with specular paths towards the SPIRE detector

Figure 7.1-2: Directions from which specularly reflected rays can hit the PACS detector.

Plot of directions towards the sky. The center of this polar diagram is the +Z axis. The circles around the +Z axis have distances of 10 degrees.

The outermost line roughly represents the limiting direction for the moon.

The limit for the earth is between the 2nd and the 3rd circle from outside.

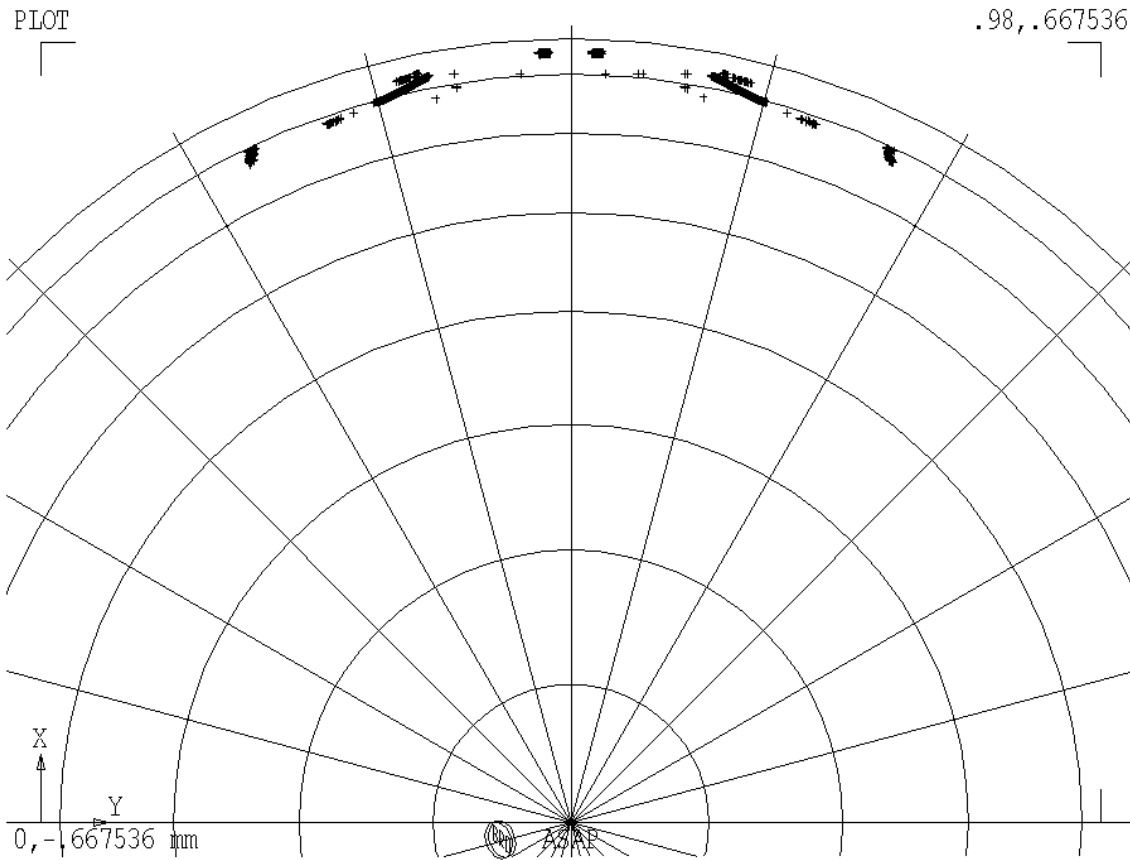Each + sign represents a direction with specular paths towards the PACS detector
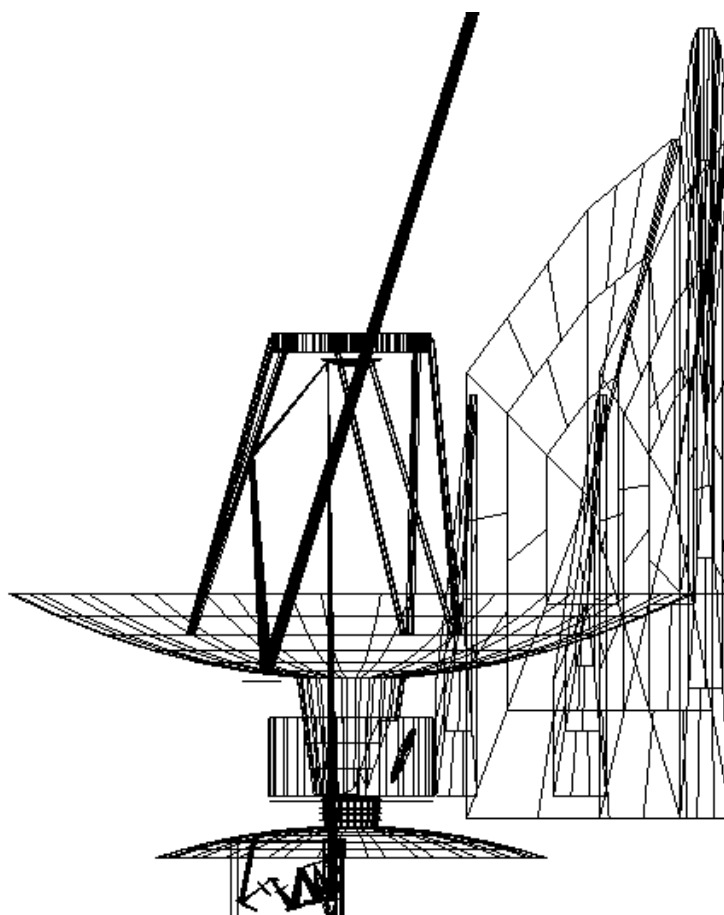
Figure 7.1-3: Specular Straylight path no. 1 for the moon
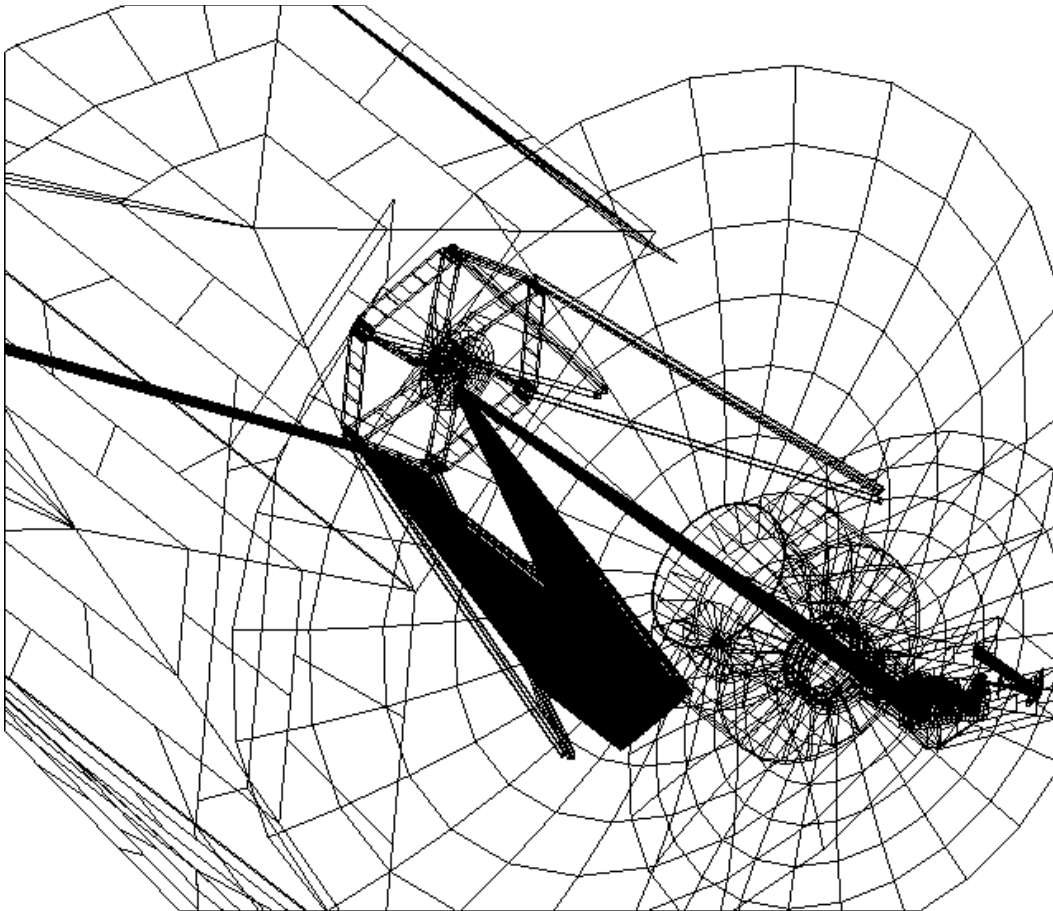
Figure 7.1-4: Specular straylight path no. 3 for the moon

Table 7.1-1 shows averaged coordinates and directions of some of the detected direct paths for the SPIRE detector. The directions are those plotted in figure 7.1-1. The coordinates are the averaged positions on Herschel, where rays on the specific path hit the first Herschel object (e.g. a hexapod strut, mirror M1, etc.).

path		coordinates of grid.			directions of source		
		X	Y	Z	A	B	C
1	**M1-Z**	**1297.47**	**284.46**	**-429.13**	**-.9189013081**	**-.2136134569**	**-.3310044862**
2	M1-Z	1297.53	-285.06	-427.56	-.9189812584	.21347118273	-.3308537199
3	**HEX-Y**	**2928.56**	**-301.65**	**237.96**	**-.9406922184**	**.13956008227**	**-.3089975805**
4	HEX+Y	2928.08	302.04	237.28	-.9406708956	-.1409893138	-.308641475

Table 7.1-1: Average coordinates and directions for the most important direct paths onto SPIRE detector

The radiation onto the SPIRE detector was calculated for paths no. 1, 2 and 3 up to now. Path 4 is symmetric to path 3, and therefore is expected to give similar results. All other paths show less radiation in the backward trace, and therefore are expected to give lower results.

Moon and Earth are treated as extended sources with angular radius of 0.002 and 0.005 rad, they are placed in a distance of 1,000,000 mm from the telescope, which is sufficient for the ASAP calculations. They are lambertian sources with emissivity 1, scattering towards the telescope targets. The Moon has such an angular extension that it covers most of the pixels of PACS and SPIRE detectors. Therefore the relative comparision to the telescope radiation is done by comparing radiances of moon and telescope and by division of the ASAP fluxes onto the detectors as in the case of self emission.

ASAP Results:

- The paths give real images on the detector. Paths 1 and 2 are somewhat diffuse, path 3 gives a sharp picture. All paths calculated up to now are potential paths for the Moon only.

- Path 1 and 2: relative flux on SPIRE detector is 1.5E-3 each

- Path 3: relative flux on SPIRE detector is 1.9E-3.

- ASAP contribution from M1 + M2 onto SPIRE detector (reference): 16.4

The contributions from these paths have to be corrected for temperature and for emissivity in order to do a correct comparision with the telescope.

- Assumed emissivity and temperature of telescope mirrors: 0.015 and 70 K each

- Assumed emissivity and temperature of the moon: 1 (black body) and 100 K for dark region, 400 K for sun illuminated region.

The ASAP contributions for all moon paths therefore have to be corrected by the following factors:

	Moon bright zone (400 K)		Moon dark zone (100 K)	
	80 µ	670 µ	80 µ	670 µ
Temperature (70 K = 1)	21.25	6.55	2.39	1.50
Emissivity	66.67	66.67	66.67	66.67
Total multiplication factor	**1417**	**437**	**159**	**100**

Table 7.1-2: Correction factors for ASAP results concernig the Moon.

The comparison to the telescope background therefore gives (in % of M1 + M2 straylight):

	Moon bright zone (400 K)		Moon dark zone (100 K)	
	80 μ	670 μ	80 μ	670 μ
Path 1	13.0%	4.0%	1.45%	0.92%
Path 2	13.0%	4.0%	1.45%	0.92%
Path 3	16.4%	5.1%	1.84%	1.16%

Table 7.1-3: Contributions from Moon on SPIRE detector for paths 1 - 3

Thus the specification of 1% is violated. The situation for PACS will be similar (this assumption has been verified independently by ALCATEL).

There are several ways to improve the situation:

- Avoid these positions by mission planning (these positions cover only a small fraction of the observable part of the sky).

- Roughening of hexapod strut surfaces:

  - difficult: to obtain really rough surfaces in the far infrared region, roughness has to be quite large, in the order of a mm

  - will increase the effective emissivity of strut surfaces.

- Rounding of hexapod strut surfaces (elliptic cross section instead of rectangular):

  - emissivity remains low

  - earth and moon straylight within specification.

Remark: The specular paths probably exist also towards other directions onto the sky due to the symmetry of the hexapod structure. There moon and earth will never appear, nevertheless planets and bright stars may reach these patches of the sky. Beam chopping and nodding will be affected. The rounding of the hexapod structures (mentioned above for the case of the moon patches) will also improve the situation for chopping and nodding.

Doc. No: HP-2-ASED-TN-0023   Page: **67**
Issue: 2   of: **73**
Date: 21.10.02   File: HP-2-ASED-TN-0023_2.doc

7.2   Scatter Paths from Moon and Earth

All results are presented as relative numbers w.r.t. the thermal radiation of the telescope mirrors M1 and M2.

Their contribution has been set to 100 so:

•   the violation of the 1% moon/earth requirement occurs if the numbers exceed 1.

The table shows that the scatter paths (scatter at primary and secondary mirror) are negligible. Thus only the patches mentioned in section 7.1 violate the specification.

Table 7.2-1: Scatter paths from moon/earth onto pacs and spire detector

emitting object	PACS DETECTOR	area= 1320 mm^2	SPIRE DETECTOR	area= 902 mm^2
	flux	irradiance	flux	irradiance
moon at 13 degrees, cone baffle	8.69E-04	8.69E-04	5.00E-04	5.00E-04
moon at 13 degrees, cylinder baffle	8.09E-04	8.09E-04	4.37E-04	4.37E-04
earth at 23 degrees, cone baffle	4.09E-03	4.09E-03	1.81E-03	1.81E-03
earth at 23 degrees, cylinder baffle	4.22E-03	4.22E-03	1.72E-03	1.72E-03

The results are those of issue 1, they have not been recalculated for the cylinder/cone baffle. Since the numbers are so low, they can be used (by similarity) for the present configuration.

7.3   Solar irradiation

The diffraction of the solar radiation at the sunshade yields irradiances small compared to the specification as elaborated in RD1.

8   Sources inside the FOV

No calculations up to now made by ASED. It has been already treated by ASEF in RD1. The results from ASEF show compliance with the specification with good margin.

9   Open Points

- The alignment cube of SPIRE is suggested to be dismountable, no decision is known up to now; this influences the geometric shape of the instrument shield near to the beams of the instruments.

- Mechanical implementation of gap closure between sunshade and M1-rim not yet consolidated.

- Calculation of specular paths across rounded strutural parts needs to be refined; this affects the paths for moon and earth and some thermal emission paths
  (AI 1 of SCI-PT/MN 14467, H/P-PDR Cryo-Optics/RF Panel Co-location meeting).

- The scattering function of SPIRE thermal filter 1 is not known.

- The very recent scattering function of the telescope mirrors is not incorporated yet (arrived after completion the calculations).

10   Summary and Recommendations

Summary for thermal self emission

The requirement of 10% is violated. The worst case situation is the small scattercone with a black cryocover resulting in 50% for PACS. For the large scattercone the numbers differ between 21% and 38% depending on how much improvement (sunshade gap) is possible and on the decision on the cryocover emissivity. Straylight aspects yield the following recommendations

- large scattercone

- reflecting cryocover

- round hexpod bar surfaces

but it is known that ground testing arguments may overrule the straylight argument in favour of the reflecting cryocover. The disadvantages of the large scattercone are more obscuration and less resolution.

Radiation from Earth and Moon

This radiation is within specification, except for small locations on the sky, where radiation reflected at rectangular hexapod structures can enter the instruments directly. These small locations exist mainly for the Moon. Only two minor paths were found which could be applicable also for the Earth (tbc). For the worst case locations of the Moon the specification is exceeded by about a factor of up to 17.

Note: Because these straylight paths partially lead to sharp ghost images on the detector, even bright stars/planets on these locations could influence chopping and nodding. There are much more dangerous locations for bright stars than for moon and earth.

Recommendation: Rounding of all affected hexapod structural elements.

Other Recommendations for SPIRE

The iterations performed during the integration of the ASAP model of SPIRE resulted in suggestions cornerning

- the SPIRE FP_UNIT (suggestion: make as much absorbing as possible)

E N D   O F   D O C U M E N T

Quantity	Name	Dep./Comp.	Quantity	Name	Dep./Comp.
	Alberti von Mathias Dr.	SM 34	X	Rühe Wolfgang	ED 6
	Barlage Bernhard	ED 11		Runge Axel	OTN/EN 64
	Bayer Thomas	ED 541		Sachsse Bernt	ED 21
X	Faas Horst	EA 65		Schäffler Johannes	OTN/EN 64
	Fehringer Alexander	SM 33	X	Schink Dietmar	ED 422
	Grasl Andreas	OTN/EN 64	X	Schlosser Christian	OTN/EN 64
	Grasshoff Brigitte	ED 521	X	Schwabbauer Paul Dr.	OTN/ED
X	Hartmann Hans Dr.	ED 422		Schweickert Gunn	SM 34
X	Hauser Armin	SM 31		Stauss Oliver	SM 33
	Hinger Jürgen	SM 31		Steininger Eric	ED 422
	Hohn Rüdiger	ED 541	X	Stritter Rene	ED 11
X	Hölzle Edgar	ED 421		Suttner Klaus	SM 32
	Huber Johann	ED 543		Tenhaeff Dieter	SM 34
	Hund Walter	SE 76		Thörmer Klaus-Horst Dr.	OTN/ED 65
X	Idler Siegmund	ED 432		Wagner Adalbert	OTN/IP 35
	Ivády von András	ACE 32		Wagner Klaus	SM 31
	Jahn Gerd Dr.	SM 31		Wietbrock, Walter	ED 521
	Kalde Clemens	ED 532		Wöhler Hans	SM 34
	Kameter Rudolf	OTN/EN 64		Zipf Ludwig	ACE 32
	Kersting Stefan	OTN/EN 63	X	Frey	ED 422
	Knoblauch August	ED 531			
	Koelle Markus	ED 533			
X	Kroeker Jürgen	ED 542	X	Alcatel	ASPI
	Kunz Oliver	SM 31	X	ESA/ESTEC	ESA
	Lamprecht Ernst	OTN/SM			
	Lang Jürgen	SE 76		**Instruments:**	
	Langfermann Michael	ED 541	X	MPE (PACS)	MPE
	Mack Paul	OTN/EN 64	X	RAL (SPIRE)	RAL
	Maier Hans-Ulrich	ED 11	X	SRON (HIFI)	SRON
	Mauch Alfred	SM 34			
X	Moritz Konrad Dr.	ED 65			
	Müller Lutz	OTN/EN 64		**Subcontractors:**	
	Muhl Eckhard	OTN/EN 64		Air Liquide	AIR
X	Pastorino Michel	ASPI Resid.		Astrium Sub-Subsyst. & Equipment	ASSE
	Peitzker Helmut	ED 65		Austrian Aerospace	AAE
	Peltz Heinz-Willi	SM 33		APCO Technologies S. A.	APCO
	Peters, Gerhard	ED 531		Astrium GmbH Space	ASIP
	Pietroboni Karin	ED 65		BOC Edwards	BOCE
	Puttlitz Joachim	OTN/EN 64		EADS CASA ESPACIO	CASA
	Raupp Helmut	SM 33		Eurocopter	ECDE
	Rebholz Reinhold	ED 541		HTS AG Zürich	HTSZ
	Reuß Friedhelm	ED 62		Linde	LIND